Ocean Engineering 310 (2024) 118758

Contents lists available at ScienceDirect

Ocean Engineering

journal homepage: www.elsevier.com/locate/oceaneng

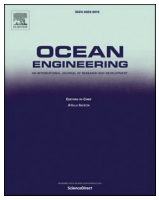

Research paper

Towards a reliable method for extrapolation of propulsion performance for vessels with twin-crp-pod system

Hanna Pruszko [a,*], Maciej Reichel [a,b], Marek Necel [c], Sören Brüns [d]

[a] Gdańsk University of Technology, Gdańsk, Poland
[b] Prof. Lech Kobyliński Foundation for Safety of Navigation, Iława, Poland
[c] Seatech Engineering Ltd, Gdańsk, Poland
[d] HSVA, Hamburg, Germany

ARTICLE INFO

Keywords:
Energy efficiency
Greenhouse gases
ITTC
CFD
Model tests
Scale error

ABSTRACT

The study presents power performance prediction of an Ultra Large Container Ship (ULCS) with hybrid twin-crp-pod propulsion system. Twin crp-pod propulsion system is a combination of three concepts: twin screw, contra-rotating propellers (crp) and conventional shaft propellers with pod propulsors behind. The presented study shows the current extrapolation method for crp propulsion systems and tries to point out its weaknesses. As a case study, a 400 m ULCS has been investigated in full-scale and in model scales of 24 and 37.416. The analyses were carried out for all scales with use of CFD numerical methods and for the scale of 37.416 based on towing tank tests. All the results have been extrapolated with the same method and results have been compared. The investigations clearly show differences in delivered power prediction extrapolated from towing tank results giving the maximum value and from CFD made to scale of 24 the minimum value. Finally, conclusions on possible sources of differences, including the numerical and analytical methods are presented.

1. Introduction

The hybrid contra-rotating-pod propulsion (Fig. 1) is a still developing solution, which combines two well-known ideas - contra rotating propellers and a pod/azimuth propulsor (Ämmälä, 2004; Ueda and Numaguchi, 2005; Sanchez-Caja, 2013; Hämäläinen and van Heerd, 2013). Major advantages of such system are seen in increased propulsion efficiency and manoeuvrability (Reichel, 2017). While minor benefits are, e.g. no need for stern thruster or less need for tug assistance in ports (Reichel et al., 2022). Additionally, crp-pod system is expected to bring about positive economic effects because there is little electric conversion loss (Shimamoto et al., 2011). Therefore, there is tendency to recognise the solution for higher energy efficiency for various types of ships.

The idea of using the single crp-pod solution to an ultra large container ship (ULCS) was presented by Kim et al. (2002). It was shown by the authors, that a gain in delivered power of 6% comparing to classic single-screw single-rudder and 10% comparing to twin-screw twin-rudder propulsion systems might be achieved.

Although, the overall gain form crp-pod propulsion is unquestionable, the challenge might be how much savings the proposed system will offer. The correct answer on that question depends strongly on the proper and reliable prediction from model tests to full scale. Here, two main issues have to be taken into account:

- scaling of pod propulsor, especially friction of the housing,
- scaling of front-aft propeller interactions - corresponding to classic contra-rotating propellers.

Unfortunately, these issues are still a challenge. On one hand, there are procedures suggested by ITTC (2017a), on the other hand towing tanks have their own extrapolation methods, but due to the lack of full scale data, all these procedures are eventually not validated. Still there are general issues to be solved, like scaling of thrust deduction fraction or specific like propeller-pod housing gap interactions.

Various approaches have been taken to solve both issues. Wang et al. (2021) investigated the difference in propulsion system for a 4000 TEU container vessels with traditional single-screw shafting propulsion and hybrid crp-pod propulsion. A numerical calculation method for the self-propulsion factors of the vessel with hybrid crp-pod propulsion was proposed by the authors using the RANS method in combination with the k-ω SST turbulence model and sliding mesh method. Regarding the

* Corresponding author.
E-mail addresses: hanna.pruszko1@pg.edu.pl (H. Pruszko), maciejr@portilawa.com, maciej.reichel@pg.edu.pl (M. Reichel), m.necel@seatech.com (M. Necel), bruens@hsva.de (S. Brüns).

https://doi.org/10.1016/j.oceaneng.2024.118758
Received 6 May 2024; Received in revised form 2 July 2024; Accepted 16 July 2024
Available online 26 July 2024

List of most important symbols

crp	contra rotating propellers
C_F	friction resistance coefficient [-]
$C_{F\ D-B}$	friction resistance coefficient for double-body simulations [-]
C_P	pressure resistance coefficient [-]
C_T	total resistance coefficient [-]
$C_{T\ D-B}$	total resistance coefficient for double-body simulations [-]
C_V	viscous resistance coefficient [-]
C_W	wave resistance coefficient [-]
D_A	diameter of the aft propeller [m]
D_F	diameter of the front propeller [m]
F_D	friction deduction force [N]
J	advance coefficient [-]
J_A	advance coefficient of the aft propeller [-]
J_F	advance coefficient of the front propeller [-]
k	form factor [-]
n_A	aft propeller revolution rate [rps]
n_F	front propeller revolution rate [rps]
K_T	thrust coefficient [-]
K_{TA}	aft propeller thrust coefficient [-]
K_{TF}	front propeller thrust coefficient [-]
$K_{TA\ CRP}$	aft propeller thrust coefficient in crp configuration [-]
$K_{TF\ CRP}$	front propeller thrust coefficient in crp configuration [-]
$K_{T0\ CPR}$	thrust coefficient of the crp system in open water condition [-]
K_Q	torque coefficient [-]
K_{QA}	aft propeller torque coefficient [-]
K_{QF}	front propeller torque coefficient [-]
$K_{QA\ CRP}$	aft propeller torque coefficient in crp configuration [-]
$K_{Q0\ CRP}$	torque coefficient of the crp system in open water condition [-]
$K_{QT\ CRP}$	torque coefficient of the crp system in condition behind the ship for the thrust identity [-]
$K_{QF\ CRP}$	front propeller torque coefficient in crp configuration [-]
K_{QT}	torque coefficient for the thrust identity condition [-]
K_{QTA}	aft propeller torque coefficient in condition behind the ship for the thrust identity [-]
K_{QTF}	front propeller torque coefficient in condition behind the ship for the thrust identity [-]
K_{Q0A}	open water aft propeller torque coefficient [-]
K_{Q0F}	open water front propeller torque coefficient [-]
R_F	friction resistance [N]
R_{S-P}	resistance in self propulsion calculations [N]
R_V	viscous resistance [N]
R_W	wave resistance [N]
t	thrust deduction fraction [-]
T_A	thrust of aft propeller [N]
T_F	thrust of front propeller [N]
Q_A	torque of aft propeller [Nm]
Q_F	torque of front propeller [Nm]
V_a	inflow velocity to the propeller [m/s]
w	wake fraction [-]
w_A	wake fraction of the aft propeller [-]
w_F	wake fraction of the front propeller [-]
λ	scale factor [-]
η_D	quasi propulsive efficiency [-]
η_R	relative rotational efficiency [-]
$\eta_{R\ CRP}$	relative rotational efficiency of the crp propulsion system [-]
η_{RA}	relative rotational efficiency of the aft propeller [-]
η_{RF}	relative rotational efficiency of the front propeller [-]
η_0	open water propeller efficiency [-]
η_{0A}	open water propeller efficiency of the aft propeller [-]
$\eta_{0A\ CRP}$	open water propeller efficiency of the aft propeller in crp configuration [-]
η_{0F}	open water propeller efficiency of the front propeller [-]
$\eta_{0F\ CRP}$	open water propeller efficiency of the front propeller in crp configuration [-]
$\eta_{0\ CRP}$	open water efficiency of the crp propulsion system [-]

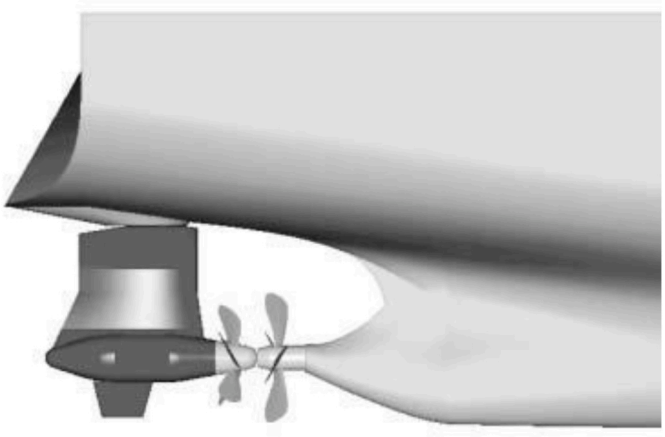

Fig. 1. Crp-pod steering-propulsion system (Ueda and Numaguchi, 2005).

method for propulsion performance analyses, the authors stated that the propulsion system should be considered as a whole unit with a fixed revolution-rate ratio (equivalent to single-screw propulsion), and multiple revolution-rate ratios must be considered.

Wang et al. (2016) carried out a hydrodynamic performance prediction of a hybrid-crp-pod propulsion system at different scales using the RANS method combined with k-ω SST turbulence model and moving mesh method. The authors analysed variations in the local flow field and hydrodynamic performance with the Reynolds number. An attempt for estimating the hydrodynamic performance of the hybrid crp pod propulsion system at full scale was proposed in the paper. Additionally, the authors introduced the idea of thrust and torque coefficients influence factor, i.e. the change of KT and KQ from open water to crp-pod conditions. It was stated that the mentioned thrust and torque coefficients influence factors of aft propeller are independent of the Reynolds number, but they indicate a nearly linear dependency with revolution ratio of the forward and aft propellers.

Similar finding was reported by Chang and Go (2011), where they mention that at constant ship speed, the revolution ratio of the forward and aft propellers uniquely corresponds to the power ratio. The authors presented also a procedure for full scale performance prediction for crp-pod. It was assumed that full scale prediction based on the forward propeller is a rational approach, due to small effect of the aft propeller on the forward propeller.

Wang and Xiong (2018) presented an integral panel method for performance analysis of hybrid contra-rotating pod propulsion system. Computations have been conducted for model scale only, however the results were compared with experimental data and show good agreement with them. The authors do not explain however the method for extrapolation and the computations for full scale have not been presented.

Xiong et al. (2016) and Wang, Xiong, and Wang (2016) reported a

particularly important phenomena, namely influence of the distance between shaft and pod propeller. Both groups involved RANS method with k-ω SST turbulence model and sliding mesh to calculate the hydrodynamic performance of crp-pod system. The main conclusion was that the thrust coefficient of the pod unit declines with the increase of axial spacing, but the trend becomes weaker, and the decreasing amplitude at lower advance coefficient is larger than that at the higher advance coefficient. An important finding was also that, the thrust coefficient and open water efficiency of the crp-pod propulsion system decrease with the increase of axial spacing, while the torque coefficient remains almost constant. The authors have not however verified the mentioned dependencies for full scale. Therefore, it is still an open question.

After all, a general conclusion might be made, that the pod unit has little influence on hydrodynamic performance of the front propeller, and the wake of front propeller has an important effect on the hydrodynamic performance of the pod unit and aft propeller, what was proved by many authors (Zhang et al., 2019; Xiong et al., 2016; Chang and Go, 2011; He and Wan, 2017).

From other point of view, an extremely critical issue was raised by Sasaki et al. (2009). The authors pointed out that, power balance of hybrid crp-pod system is the most important and it should be varied depending on a course keeping ability of the design ship. Such an approach may be crucial for ship handling and navigational safety, and it has to be known if and how much the mentioned balance will change during extrapolation from model to full scale.

An interesting fact on the crp-pod propulsion system has been discovered by Zhang et al. (2020). The authors namely carried out CFD computations at behind-hull conditions and concluded that, the existence of the forward propeller reduces the average aft blade load and results in a shift of the phase angle corresponding to the load peak.

Finally, Reichel et al. (2022) presented the crp-pod propulsion system upgraded to a twin-crp-pod system on an Ultra Large Container Ship (ULCS). The authors presented challenges related to such a propulsion system and equipment arrangement that might be crucial in the design phase. They concluded, that, the use of a twin-crp-pod solution in the case of Ultra Large Container Ships might be an excellent answer to present and coming environmental regulations, although some drawbacks have to be overcome.

Taking the above-mentioned research into account, a clear view on their weaknesses shows up. Nevertheless, none of these papers takes all challenging phenomena into account, as they focus on separate issues. Therefore, the overall aim of this paper is to find and summarise the most probable places in the existing extrapolation methods, which may result in most significant errors during full scale propulsion prediction.

2. Propulsion performance prediction in crp-pod system

Nowadays it is rather common, that experimental and numerical methods are considered equally reliable in prediction of resistance, open water propeller hydrodynamic characteristics and eventually propulsion performance both for single-propeller and twin-propeller ships (Pruszko et al., 2023a, 2023b). The crp-pod propulsion arrangement is however unique solution, where specific, sophisticated interactions especially between propellers are present. Some of the state-of-the-art analysis methods could have, therefore, weaknesses, especially in prediction of full scale performance. Below, brief summary on experimental and numerical approach to the crp-pod hydrodynamic issue.

2.1. Model testing of propulsion performance in crp-pod system and extrapolation methods

Taking into account the complexity of crp-pod propulsion configuration and interactions present in the system, much wider testing campaign, comparing to single-propeller single-rudder has to be carried out. The 28th ITTC Propulsion Committee (ITTC, 2017b) issued a guideline on Hybrid Contra-Rotating Shaft Pod Propulsors Model Test, where a testing procedure for tank experiments is given. Besides bare hull resistance test, which in principle is conducted in the same way as for ships with any other steering-propulsion system, a set of five propulsor open water tests is intended to be done, later on followed by self-propulsion tests.

Fig. 2 shows the types of open water tests, which have to be carried out to properly evaluate the performance of crp-pod system. Tests A and C are the conventional propeller open water tests and test D is the conventional podded propulsor open water test. Although tests C and D are not compulsory, they can be conducted to evaluate interactions between pod housing and propeller and of contra-rotating propellers on the pod housing open water test characteristics. Test B is required for taking into account the influence of dynamometer wake on propeller characteristics on test E.

In order to determine more accurate propeller open boat wake fraction, reverse propeller open boat with dummy shaft behind the propeller, as in Fig. 3 is beneficial.

Subsequently, the self-propulsion model tests have to be carried out according to commonly used ITTC procedure with further scaling of wake fraction, propeller open water characteristics and pod housing drag.

As mentioned earlier, there are two key issues regarding the extrapolation of crp-pod system. The first one - interactions between propellers and the later one - scaling of friction of pod housing in front

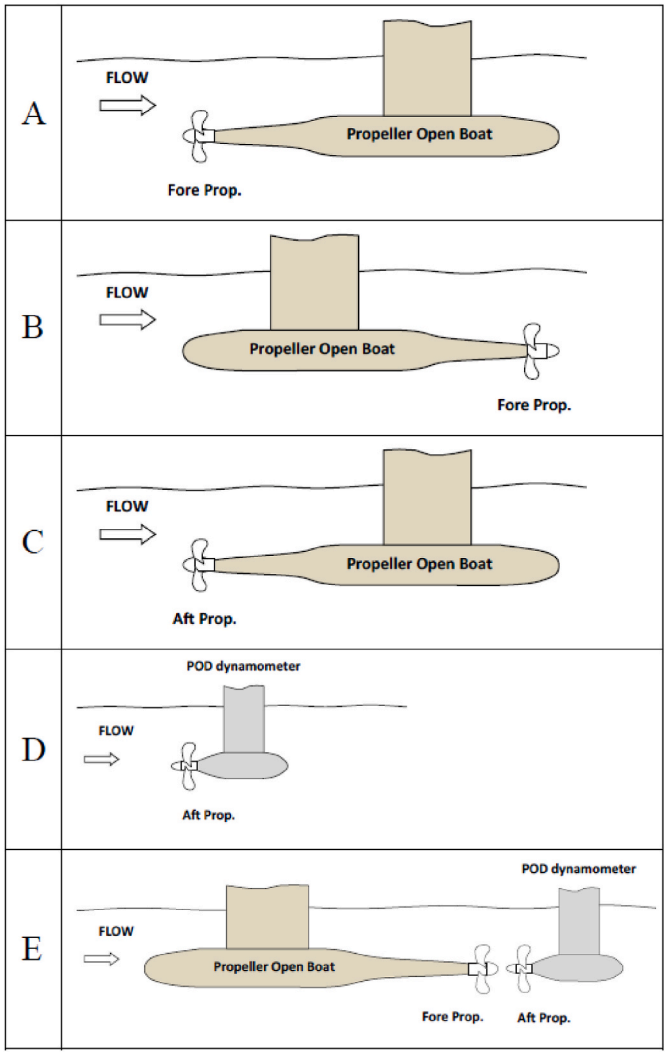

Fig. 2. Open water test configurations for crp-pod arrangement (ITTC, 2017b).

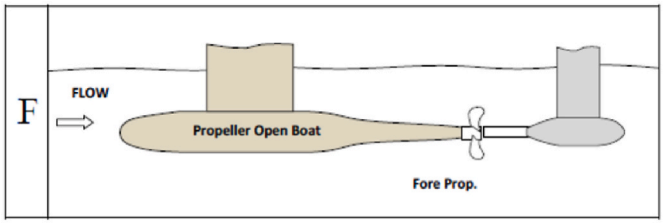

Fig. 3. Additional test configuration (ITTC, 2017b).

propeller wake. Both challenges are now managed rather cursorily, as shown below.

To predict the full scale performance of the crp from model tests, the equivalent single-propeller approach using the classic non-dimensional coefficients has been widely used (van Manen and Oosterveld, 1968):

$$J_a = V_a/n_F D_F \tag{1}$$

$$K_{T\ CRP} = \frac{T_F + T_A}{\rho n_F^2 D_F^4} \tag{2}$$

$$K_{Q\ CRP} = \frac{n_F Q_F + n_A Q_A}{\rho n_F^3 D_F^5} \tag{3}$$

where ρ, V_a, n, D, T, Q, J_a, $K_{T\ CRP}$, $K_{Q\ CRP}$ represent the water density, advance velocity, propeller revolution, propeller diameter, thrust, torque, advance ratio, thrust, and torque coefficients of the propulsion system. Subscripts "F'' and "A'' signify the front and aft propeller, respectively. This method, combined with ITTC-78 extrapolation of single-propeller self-propulsion tests is relatively straightforward and can predict the overall performance of crp system, but has two main drawbacks (Chang and Go, 2011):

- this approach cannot evaluate the load and revolution of the aft propeller, which can be driven regardless of the front propeller
- self-propulsion factors in this approach are not for the actual front and aft propellers, but for imaginary propellers with equivalent loads. Therefore, these factors do not give practical information for propeller design

For the extrapolation of podded propulsors, 25th ITTC Specialist Committee on Azimuthing Podded Propulsion (ITTC, 2008) has proposed a unified approach. This method splits the pod unit into the podded propeller and the pod housing and then corrects both of them. The standard ITTC-78 extrapolation procedure is used for the correction for podded propeller, while the form factor approach is used for the pod housing resistance. This method is based on empirical formulas and needs to be verified against many propellers at full scale.

The whole approach, both for open water testing and extrapolation method have some significant weaknesses and uncertainty sources:

- unknown actual influence of propeller open boat on the wake and interaction between propellers (configuration E),
- change of actual blade angle of attack of aft propeller,
- pod housing friction.

The drawbacks of the abovementioned ITTC procedure are clear, therefore there are attempts to elaborate a prediction procedure, which covers all the necessary phenomena. Some procedures, slightly differing between each other were presented by Chung and Go (2011), Wang et al. (2016) and Quereda et al. (2017).

All these alternative procedures have one main factor in common, i.e. they predict the propulsion performance of both propellers separately. But to do so in a reliable way, the knowledge of complicated hydrodynamic performance of both propellers is necessary, which sometimes are recognisable only through the numerical simulations.

2.2. Direct CFD full scale propulsion prediction

Numerical simulations seem to offer a very interesting alternative to the towing tank testing in terms of investigation into scale effect. Since it allows to perform calculations in multiple scales, including also full scale simulations it can be a source of the knowledge that cannot be gained from the model testing. Extremely valuable, but also still rare are the publicly available results of the full scale sea trials supplemented with the ship hull shape data, roughness measurements and precise data about sea trials condition. This can serve as a validation to full scale numerical simulations, which remains uncertain without high quality sea trials results. Despite such limitations, multiple scientists see the advantages of the full scale numerical simulations, and similar approach has been taken in presented study.

A well-known benchmark database was obtained during Lloyd's workshop which included full scale trials of general cargo carrier REGAL. The experimental and full scale CFD calculations were presented by Ponkratov and Zegos (2015); Ponkratov (2017). Those results were also used to validate the full scale self-propulsion simulations carried out by Jasak et al. (2019). The calculations were performed with the propeller modelled as an actuator disc. The obtained results matched well sea trials output. Findings from Lloyds workshop were also used to some full scale CFD simulation guidelines for model calibration (Huang et al., 2023; Krasilnikov et al., 2023). The self-propulsion calculations for KCS with various propulsion models were described by Yu et al. (2021). Moreover, the comparison of the full scale calculations to various extrapolation methods were presented. Sun et al. (2020) performed model scale and full scale CFD calculations with and without free surface (double body simulations) and compared it to towing tank and sea trials data. Also, various corrections for hull roughness and correction for the propeller performance in double body simulations were checked. Similar approach for the double body self-propulsion simulation were presented by Mikkelsen et al. (2019). Recently, the impact of hull roughness and hull imperfections on the performance in the ship scale were the subject of the deeper interest (Mikkelsen and Walther, 2020; Quist et al., 2023). It was concluded that taking into account the effect of hull and propeller roughness can significantly improve the accuracy of the predictions yielding credible and high-quality calculations results.

Moreover, the CFD simulations are commonly used to investigate scaling methods and extrapolation procedures by comparison extrapolated values to direct propulsion calculations. Well conducted CFD calculation can give an insight into some of the flow field characteristics which are difficult to capture in actual conditions and at multiple Reynolds number values. It has been already proved by several authors that the ship form factor, which for Hughes & Prohaska extrapolation method is assumed constant for model and ship, actually is scale dependent (Dogrul et al., 2020; Terziev et al., 2019; 2021). Another aspect of CFD self-propulsion analysis is scaling of propeller characteristics. The multi-scale calculations were performed and compared by Khraisat et al. (2023). In general, such type of calculations can help to understand better the differences in propulsion characteristics in various scales.

3. Aim and scope of current research

In the present paper, the propulsive characteristics of an Ultra Large Container Ship (ULCS) are studied numerically. Based on this study, some considerations on propulsive performance prediction and extrapolation method for ships equipped with hybrid crp-pod propulsion systems are presented. Specifically, the overall aim of the research is to find the most probable places in the existing extrapolation methods, which may result in most significant errors during full scale propulsion prediction. Therefore, a multi-directional approach for model and full scale testing and numerical calculation according to Table 1 is taken. Taking into account various sources of inaccuracies, a set of comparisons

Table 1
Analysed types of tests/computations.

	Scale λ	1	24	37.416
Model tests	Resistance	–	–	+
	Propeller open water	–	–	+
	Self-propulsion	–	–	+
	Extrapolation	–	–	+
CFD computations	Resistance	+	+	+
	Propeller open water	+	+	+
	Self-propulsion	+	+	+
	Extrapolation	–	+	+

covering particular phases of extrapolation process has been made to check the level of possible difference in full scale prediction.

To partially capture the scale effect, two model scales have been chosen for computations - 37.416 and 24. The scale of 37.416 was chosen for the purpose of validation of the resistance calculation against the HSVA towing tank tests, while the scale of 24 due to further calculations of manoeuvring forces, that are validated against free-running model tests with manned model at Ship Handling, Research and Training Centre in Iława, Poland. For both analysed scale factors, the extrapolated results from CFD and tank tests have been compared to each other. Additionally, full scale CFD computations have been performed.

The scope of numerical simulation included therefore:

- Calm water resistance for the design speed of 21 knots (corresponding to 2.205 m/s in scale $\lambda = 24$ and 1.766 m/s in model scale $\lambda = 37.416$) to determine the total resistance of the hull – **model** scales and **full** scale
- Propeller open water propeller hydrodynamic characteristics - **model** scale and **full** scales for crp configuration and for separated propellers
- Double-body resistance for the design speed of 21 knots (corresponding to 2.205 m/s in scale $\lambda = 24$ and 1.766 m/s in model scale $\lambda = 37.416$) to determine the viscous resistance and calculate wave resistance as a difference between total resistance and viscous resistance – **model** scales and **full** scale
- Double-body self-propulsion– for the design speed of 21 knots (corresponding to 2.205 m/s in scale $\lambda = 24$ and 1.766 m/s in model scale $\lambda = 37.416$) with constant ratio of revolution between front and aft propellers to determine thrust and torque of the propellers, as well as resistance of the appended ship in self-propulsion condition – **model** scales and **full** scale

Four different set-ups of numerical simulations were applied: to evaluate open water propeller characteristics, resistance in calm water with and without free surface, and to find the ship/model self-propulsion point. All those simulations are necessary to determine the self-propulsion coefficients that are also interest of this study. The differences in numerical setup included mesh, temporal discretisation, and computational domain size. Following subsections aim to describe the set-up of each simulation type in details.

4. Case study vessel

The case study vessel is a 400 m Ultra Large Container Ship (ULCS). The hull shape has been obtained by redesigning a single screw ship, keeping the entrance and parallel middle body unaffected. The decision process and redesign objectives were described in detail by (Reichel et al., 2022). Table 2 presents the main particulars of the case study vessel. The 3D model of the case study vessel is presented in Fig. 4.

The pod housings were designed based on the analysis of the currently available market solutions, while the propellers, after a comprehensive review, were taken from the stock of Prof. Lech Kobyliński Foundation for Safety of Navigation (front propeller) and Gdańsk

Table 2
Main particulars of the case study vessel.

Quantity	Symbol	Value		
Scale	λ	1	24	37.416
Length overall	LOA [m]	399.90	16.663	10.110
Length between perpendiculars	LPP [m]	378.40	15.767	10.690
Breadth moulded	B [m]	53.60	2.233	1.433
Drought (design)	T_D [m]	14.00	0.583	0.374
Displacement	∇ [m^3]	199068	14.400	3.800
Wetted surface	Ss [m^2]	25965	45.08	18.55
Service speed	Vs [m/s]	10.8 [21 kn]	2.205	1.766
Froude Number	F_N [-]		0.1737	
Reynolds Number	R_N [-]	$3.588 \cdot 10^9$	$3.179 \cdot 10^7$	$1.680 \cdot 10^7$

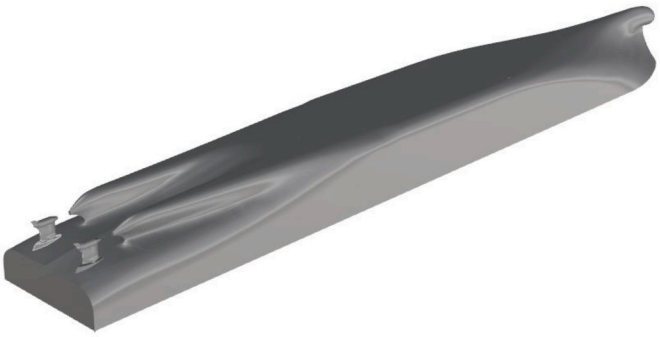

Fig. 4. Geometry of the analysed ULCS.

University of Technology (aft propeller).

Fig. 5 presents the pod housing and propellers 3D models. The propeller geometric characteristics are summarised in Table 3. It has to be noted, that the ratio of aft to front propeller diameters was assumed as 0.78. The ratio has been chosen based on simplified propeller momentum theory to achieve the highest utilisation of front propeller axial losses, thus, to work most efficiently in a slipstream of the front propeller.

5. Methods

5.1. Computational fluid dynamics

Numerical methods allow to solve discretised governing equations of mass, momentum and energy conservation that are commonly known as

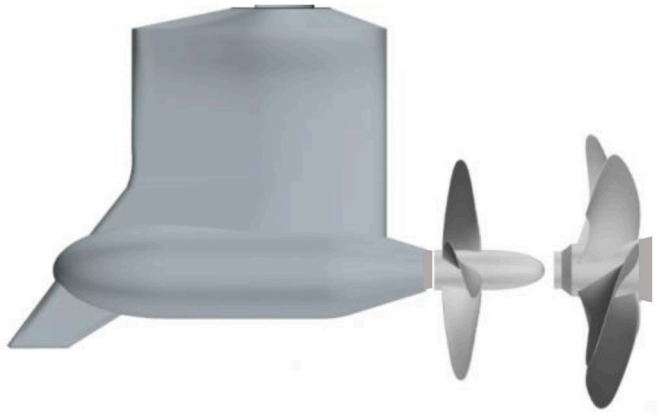

Fig. 5. Geometry of the crp-pod propulsion system.

Table 3
Propeller geometry characteristics for full and model scale.

Quantity	Symbol	Front propeller			Aft propeller		
Scale	λ	1	24	37.416	1	24	37.416
Diameter	D [m]	7.680	0.320	0.205	6.000	0.250	0.160
Number of blades	z [-]	5			4		
Pitch Ratio	$P_{0.7}/D$ [-]	1.0221			1.016		
Expanded area ratio	A_E/A_0 [-]	0.8014			0.5184		
Rotating direction (open water)		left			right		
Rotating direction (self-propulsion)		inwards			outwards		

Navier-Stokes equations. Depending on problem complexity, different simplifications might be applied. For naval applications, where the fluid is assumed to be incompressible, only mass and momentum continuity is considered. Nowadays, the most commonly applied method is the Finite Volume Method. It involves discretisation of the computational domain surrounding the object of interest, in this case a ship, and iteratively solves governing equations in every mesh cell.

The most popular are turbulence models, based on Unsteady Reynolds Averaged Navier-Stokes Equations (URANS). The method is based on the assumption that instantaneous velocity might be represented in terms of mean and fluctuating components. Those values are inserted into Navier-Stokes equations are then averaged. The process of averaging causes an additional, previously unknown term – Reynolds stress – to appear in the equations and it is written as follows:

$$\frac{\partial(\rho\overline{u_i})}{\partial x_i} = 0 \tag{4}$$

$$\frac{\partial(\rho\overline{u_i})}{\partial t} + \frac{\partial}{\partial x_j}\left(\rho\overline{u_i}\overline{u_j} + \rho\overline{u_i'u_j'}\right) = \frac{\partial\overline{p}}{\partial x_i} + \frac{\partial\overline{\tau_{ij}}}{\partial x_j} \tag{5}$$

where p is pressure, ρ is fluid density, $\rho u_i' u_j'$ are Reynolds stresses, u_i' are averaged components of velocity vector in the Cartesian system of coordinates, and τ_{ij}' are the mean viscous stress tensor components and are defined as follows:

$$\overline{\tau_{ij}} = \mu\left(\frac{\partial\overline{u_i}}{\partial x_j} + \frac{\partial\overline{u_j}}{\partial x_i}\right) \tag{6}$$

In order to close the new system of equations, the Reynolds stresses tensor needs to be modelled using a turbulence model. Over the years, many turbulence models have been defined and it requires some knowledge and experience from the user to choose and specify it correctly.

To perform CFD calculations, STAR CCM + software was used. The solver uses Finite Volume Method. Different simulation set-ups and mesh types has been used to study various aspects of resistance and propulsion performance and they are described in the following sections.

For each simulation case, the k-ω SST model with all y + wall treatment was selected. This helps to combine two approaches: direct resolution of the viscous layer for cells with y + below 5, application of the logarithmic law function for cells with y + above 30 and blending these two approaches for the cells inside the buffer layer. The dimensionless velocity u+ is then calculated as:

$$u^+ = \frac{1}{\kappa}\ln(1+\kappa y^+) + C\left(1 - e^{-\frac{y^+}{y_m^+}} - \frac{y^+}{y_m^+}e^{-by^+}\right) \tag{7}$$

Where C and b are defined as:

$$C = \frac{1}{\kappa}\ln\left(\frac{E}{\kappa}\right) \tag{8}$$

$$b = \frac{1}{2}\left(y_m^+\frac{\kappa}{C} + \frac{1}{y_m^+}\right) \tag{9}$$

and E is the log law offset equal to E = 9, κ = 0.42 - von Kármán constant, and y_m^+ corresponds to the theoretical intersection of the viscous sub-layer and the log-layer solution (Siemens PLM Software, 2022). Additionally, for model scale calculations the gamma transition model was used.

The flowchart of the study is presented in Fig. 6. It was noticed that self-propulsion calculations with the free surface are characterised by large variations of forces giving significant numerical uncertainty. Therefore, it was decided to perform the self-propulsion simulations in the condition without the free surface (double body self-propulsion simulation).

The calm water calculations and double body calculations were performed to determine the wave resistance of the tested vessel. The self-propulsion simulations were performed for single phase flow, however, the wave resistance was added, to obtain more accurate prediction of the self-propulsion point. Moreover, for model scales the friction deduction force was added. The open water propeller calculations of separate propellers and in contra-rotating condition allows to determine the elements of propulsion efficiency.

5.1.1. Calm water simulation

For calm water simulations with free surface the flow was modelled as multiphase, turbulent, and unsteady. In order to capture the interface between phases, a surface capturing VOF (Volume of Fluid) model was applied. For spatial discretisation, a second order, upwind numerical scheme was used for convection term and to compute motions of a ship as a response to fluid forces, the model of DFBI (Dynamic Fluid Body Interaction) was applied.

The setup of the numerical domain is presented in Fig. 7 and Table 4. The size of the domain and the ship position was specified in order to avoid reflection from the side and downstream boundary and also to capture the Kelvin wave pattern. Additionally, to minimise the reflections of waves on the side and outlet boundaries, numerical wave damping was applied. The damping zone each time had half the length of the model and damping was applied on the side and outlet boundaries.

The discretisation of the volume was performed according to ITTC recommendations (ITTC, 2014). Standard refinements in the areas of free surface, wake and near the hull were applied (Fig. 8). Mesh resolution in the region of the ship boundary was slightly various for different scales. For both model scales the y+ was kept below 2 aiming to obtain as similar averaged wall y + over the hull surface as possible, 14 prisms were used with the stretch factor of 1.5. For scale of 37.416 the thickness of prism layer was equal to 0.03 m, and for scale of 24 the thickness of prism layer was equal to 0.02 m. Due to significant problems with the stability of calculations the viscous layer was not resolved directly for full scale ship, and averaged y+ was kept below 50. For full scale the thickness of the prism layer was equal to 0.2 m and 16 prisms were used with the stretch factor equal to 1.3. Moreover, obtaining y + for the full scale vessel would result in very significant number of cells (Stern et al., 2013; Terziev et al., 2019). The disadvantage of such decision is introducing some uncertainty due to various values of y+, not only the scale error and Reynolds number.

It was also necessary to refine the mesh for the full scale ship, also

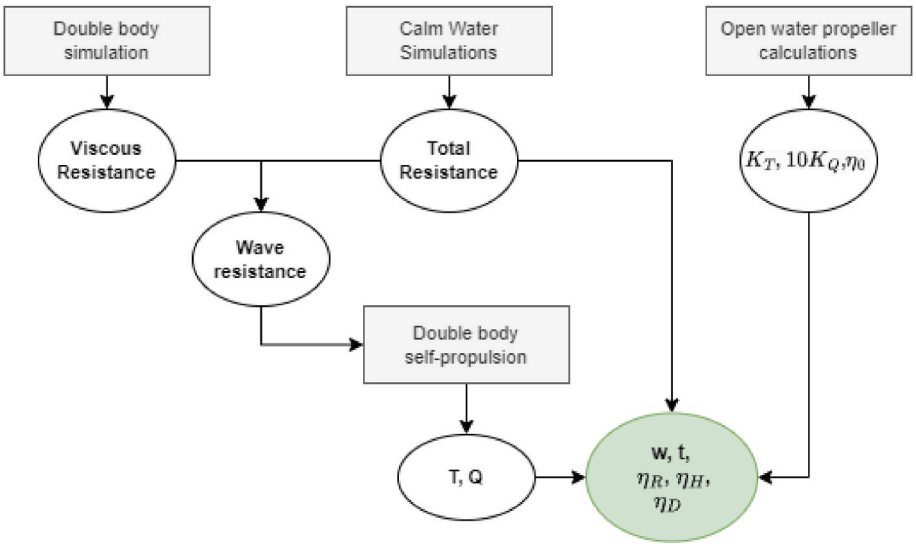

Fig. 6. Procedure for elaboration of propulsion coefficients.

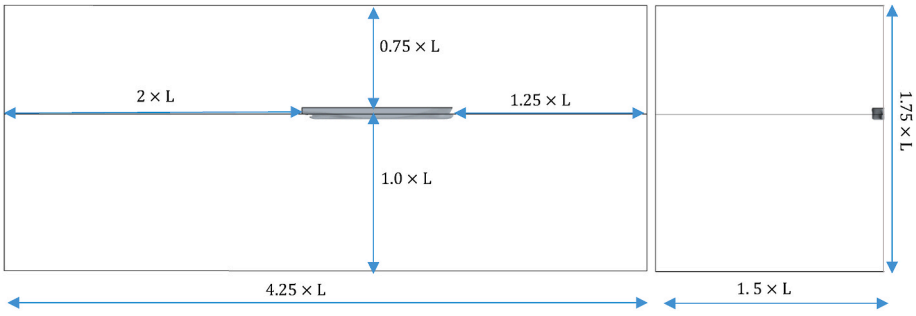

Fig. 7. Setup of a numerical domain for the CFD simulations (ship resistance on calm water).

Table 4
Setup of a numerical domain for the CFD simulations (ship resistance on calm water).

Boundary	Boundary Condition
Upstream	Velocity inlet
Downstream	Pressure outlet
Side	Symmetry plane
Symmetry	Symmetry plane
Top	Velocity inlet
Bottom	Velocity inlet

due to calculation stability reasons. For model scale meshes the total cell count was equal to 5.1 M, whereas, for the full scale ship it was equal to 6.9 M. Verification study was carried out for model scale ($\lambda = 37.416$) for one coarser and one denser mesh, with a total cell number equal to 2.9 M for coarsest mesh and 14.7 M cells for finer mesh. Verification followed the Generalised Richardson Extrapolation Method (ITTC, 2021b)ITTC, 2017. Base size of element was systematically changed by the factor of $\sqrt{2}$ in X, Y and Z direction in each mesh. Differences in obtained value of total resistance between the base and fine mesh was equal to −1.46%. Thus, it was decided to use base mesh having 5.1 M cells instead of the finest. Results of verification study was presented in Table 5 in Section 5, where mesh one corresponds to the finest grid and mesh three to the coarsest mesh.

The first order temporal discretisation was used for the calm water simulations. The time step of the simulations was adjusted to not exceed Convective Courant Number by five for the vast majority of the cells on the free surface. Additionally, to avoid numerical ventilation the HRIC scheme was used (Gray-Stephens et al., 2021).

Results obtained by the CFD simulations were verified and validated against towing tank results. In Tables 5 and 6 the verification and validation study results for the model scale of 37.416 is presented.

Validation uncertainty is the root of the squared data and simulation uncertainty sum. Fig. 9 shows the dependence of the resistance components on the mesh size, where C_T corresponds to total resistance coefficient, while C_F and C_P to friction and pressure resistance coefficients, respectively. According to Fig. 9, the total resistance components are converging in a monotonic manner. Moreover, we can see that the value of the friction resistance coefficient is significantly changing between mesh two and mesh three.

5.1.2. *Double body simulations*

The double body simulations were performed for similar numerical setup as the calm water simulations. The differences included of course the definition of the top boundary. It was positioned at the level of the ship waterline and the symmetry plane boundary condition was prescribed to it. Remaining boundaries were kept the same as described in Section 5.1.1. The flow was modelled as a single-phase flow. The time step was the same as for free-surface calm water simulation. To exclude the influence of the mesh, the underwater mesh part was kept the same, without introducing refinements of coarsening. It resulted in the mesh which is not “optimised” for this purpose, but it is believed, it allowed for an accurate estimation of the wave resistance. Fig. 10 presents the numerical mesh used for the double-body simulations; the one half was mirrored in this figure for better mesh visualisation.

The total number of mesh elements was equal to 3.6 M cells for scales

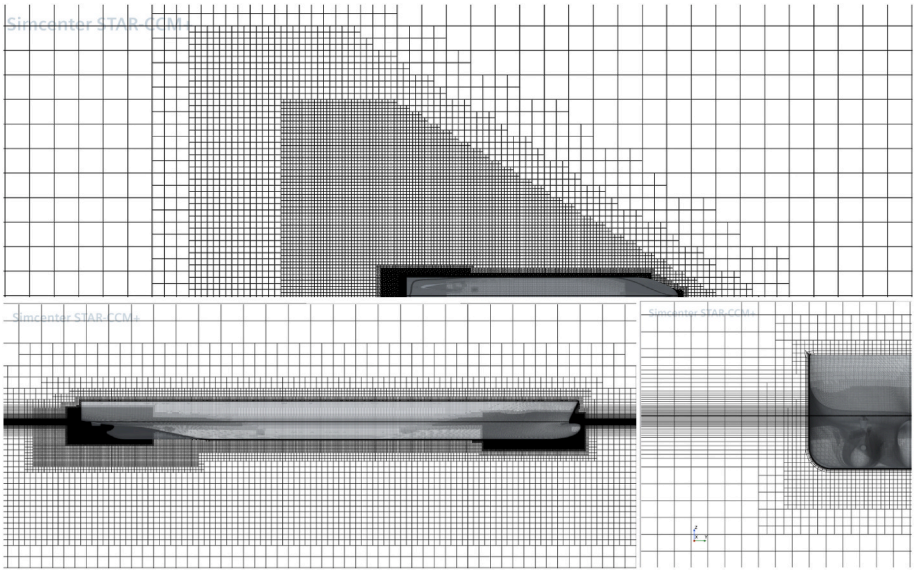

Fig. 8. 2D views on full scale generated mesh.

Table 5
CFD verification study for the model scale λ = 37.416.

Grid refinement ratio R_G [-]	Order of accuracy P_G [-]	Correction factor C_G [-]	Grid size error δ_G^* [-]	Grid size uncertainty U_G [%]
0.157	5.348	0.74	$4.60 \cdot 10^{-6}$	0.18

Table 6
CFD validation study for the model scale λ = 37.416.

Error E [%]	Validation uncertainty U_V [%]	Data uncertainty U_D [%]	Numerical simulation uncertainty U_{SN} [%]
4.49	0.82	0.8	0.15

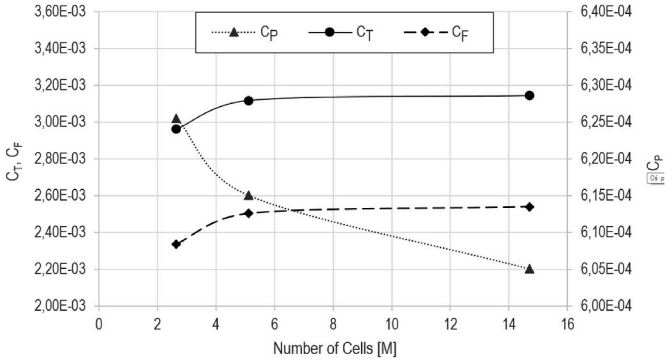

Fig. 9. Convergence of the resistance coefficients.

λ = 37.416 and λ = 24, whereas for the full scale calculations it was equal to 5.5 M cells.

Performing both double body and free surface calm water simulations allowed to obtain valuable information about different components of total resistance. There are several ways to decompose the ship total resistance, and according to ITTC it can be done as:

$$C_T = (1+k)C_F + C_W \tag{10}$$

where: C_T, C_F and C_W are coefficients of total, friction, and wave resistance, respectively. For the double body simulations, the wave resistance does not exist ($C_W = 0$) therefore the total resistance in double body simulations can be written as:

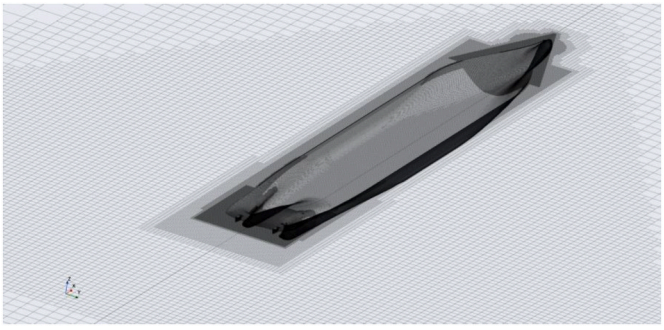

Fig. 10. Mesh for the full scale double body simulations.

$$C_{T\,D-B} = (1+k)C_{F\,D-B} = C_V \tag{11}$$

where: C_V is the viscous resistance coefficient, which corresponds to total resistance in the double body simulations, k is the form factor, and it can be derived from the numerical simulations according to the equation:

$$(1+k) = \frac{C_{T\,D-B}}{C_{F\,D-B}} \text{ or } (1+k) = \frac{C_V}{C_{F\,D-B}} \tag{12}$$

Any force coefficient multiplied by the term $0.5\rho V^2 S$, where V is the ship/model velocity, S the ship/model wetted surface and ρ the water density, gives the dimensional value of the force, in our case this are various components of total resistance. In present study the values of the wave resistance R_W were determined as the difference between total resistance for simulations with the free surface R_T and viscous resistance from double-body calculations R_V according to the formula:

$$R_W = R_T - R_V \tag{13}$$

The values of the wave resistance are further used in self-propulsion simulations to determine the self-propulsion point.

5.1.3. Open water propeller simulations

Two types of open water simulations were performed to determine the hydrodynamic characteristics of each propeller operating separately, and in contra-rotating manner. Both types of calculations were performed in full scale and in model scales $\lambda = 24$ and $\lambda = 37.416$.

The flow was single phase and turbulent. For model scales the k-ω SST turbulence model with gamma transition was used. For propellers working separately the steady solver with moving reference frame approach was selected. On the contrary, the open water propeller characteristics in contra-rotating (crp) configuration was determined using unsteady second order solver. It was decided to use different solvers, because no significant differences between steady and unsteady solver are expected for the standard separate open-water propeller characteristics determination. This choice helps to reduce the computational time. For the open water propeller characteristics in crp condition, the time step was selected to satisfy the condition of 1 degree of rotation per time step, based on the revolution of the aft propeller. The sliding mesh approach was used for the simulations of the propellers in crp configuration.

The calculations were run for the values of advance coefficient $J = \frac{V_a}{nD}$ between 0.3 and 1. The calculations were done for propeller rate of revolution corresponding to the same revolutions as determined in self-propulsion simulations as the propulsion point. – see Table 9. This allowed to minimise the influence of the difference in Reynolds number on the propeller characteristics in open-water and self-propulsion conditions. Described setup corresponded to the range of propeller Reynolds number between $1.4 \cdot 10^5 \cdot$ and $2.25 \cdot 10^5$ for the scale of 37.416, between $2.78 \cdot 10^5$ and $4.28 \cdot 10^5$ for the scale of 24 and between $3.58 \cdot 10^8$ and $5.46 \cdot 10^8$ for the full scale. For the crp simulations the advance coefficient was calculated based on the parameters of the front propeller. The constant revolution and variable inlet velocity approach was applied. The revolutions of the propellers have been chosen to match similar range of the propeller Reynolds number as for the self-propulsion simulations. For the crp configuration the rate of revolution between aft and front propeller was set to $n_A/n_F = 1.366$. This choice is explained later in Section 6.3

The numerical domain had the length of 12D, height and width of 6D. The propeller was placed in the middle of the domain. The upstream and downstream boundaries had prescribed the velocity inlet and pressure outlet boundary conditions, respectively. Remaining boundaries had a symmetry plane condition. The rotating region had a dimension of 1.6D and the internal interface boundary was prescribed on the surface of the cylinder that formed the rotating region. The computational domain for the front propeller is presented in Fig. 11.

Two types of meshes were used for the calculation. The polyhedral mesh was used in the rotating region, and trimmed mesh in the static region. The mesh coarsening was applied in the outside boundaries, while the finer mesh was applied at the region around the propeller. For model scale simulations the wall y+ was kept below 2 on the surface of the propeller blades. For full scale propeller simulations, the y+ was approximately 40. For all scales six prisms and stretch factor of 1.5 were used. The thickness of the prism layer was equal to $5.0 \cdot 10^{-4}$ m for model scales, and 0.003 m for full scale. Moreover, it was also necessary to decrease the base size of the mesh element on the propeller blade for the full scale crp calculations for the stability of the calculations. The propeller tips and blades leading edge were treated with the special attention to ensure the accurate representation of the propeller geometry. To do so, the minimum size of element was equal to 1 mm for the full scale simulations, and $5 \cdot 10^{-5}$m for the model scale simulations. Mesh for open water propeller simulations is presented in Fig. 12.

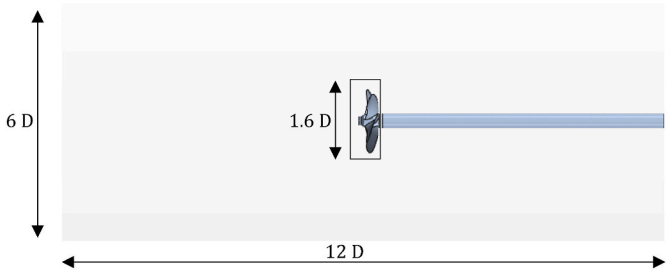

Fig. 11. Domain for the open water propeller calculations. Depicted: full scale front propeller.

Described condition resulted in the number of mesh elements for propellers tested separately between 3.8 M cells and 4.2 M cells for pod propeller, and between 5.4 M cells and 6.12 M cells for shaft propeller. In crp configuration the total number of elements was between 7.5 M and 8.7 M cells.

5.1.4. Self-propulsion simulations

The self-propulsion simulations were a combination of numerical setups and meshes of the previously described simulations. The flow was turbulent, single-phase (no free surface) and unsteady. The temporal solver and time step was the same as in crp calculations. Similar to previous resistance simulations for the reduction of the computational expenses these simulations were run just for the half of the hull and one set of the propellers. Therefore, the symmetry boundary condition was assigned on the symmetry plane of the hull. For the rotating region bounding the propellers the sliding mesh was used. The interface boundary condition was applied on the surfaces of cylinders that were the outside boundaries of the rotating regions.

The calculations were performed for the constant ratio of the front and aft propeller revolution. The propeller revolution rate was selected based on the optimisation study performed for the model scale $\lambda = 37.416$.

The propeller revolutions $n_A/n_F = 1.366$ based on the criterion of minimum delivered power of the propellers has been choosen.

The self-propulsion calculations aimed to find the self-propulsion point. It was assumed that it is reached when the condition described in Eq. (14) is satisfied:

$$2(T_F + T_A) - R_{S-P} - R_W = F_D \tag{14}$$

where:

T_F – Thrust of the front propeller [N].

T_A – Thrust of the aft propeller [N].

R_{S-P} – Resistance in the self-propulsion condition [N].

R_W – Wave resistance in the calm water simulation [N], defined as in Eq. (10):

F_D – Friction deduction force [N].

The term R_W is added to Eq. (8) in order to get estimation, which would correspond to the condition with the free surface propulsion test. The friction deduction force is calculated each time for model scale self-propulsion calculations. It was equal to 45.94 N for the model scale of 37.416, and 135.63 N for the model scale of 24. The friction deduction force was calculated according to HSVA internal power prediction procedure.

The calculations were conducted similarly to model tests for two points – one, which corresponded to thrust deficit, and the second which corresponded to thrust overload. The self-propulsion point was obtained from the linear interpolation between those two points. The direct results of the self-propulsion calculations were propeller revolutions, together with thrust and torque for both propellers. The general ITTC-78 Performance Prediction Method shown in Fig. 13 was followed to obtain values of propulsion coefficients values.

Finally, the thrust deduction fraction t was calculated according to formula:

$$t = 1 - \left(\frac{R_T - F_D}{2(T_F + T_A)} \right) \tag{15}$$

And quasi-propulsive efficiency η_D can be defined as:

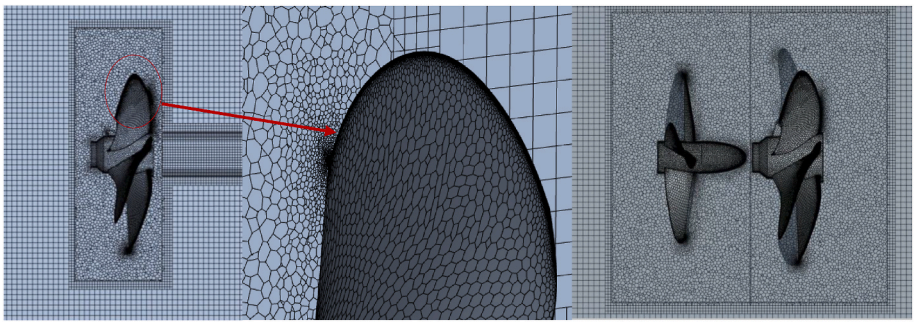

Fig. 12. Mesh for the open water propeller calculations.

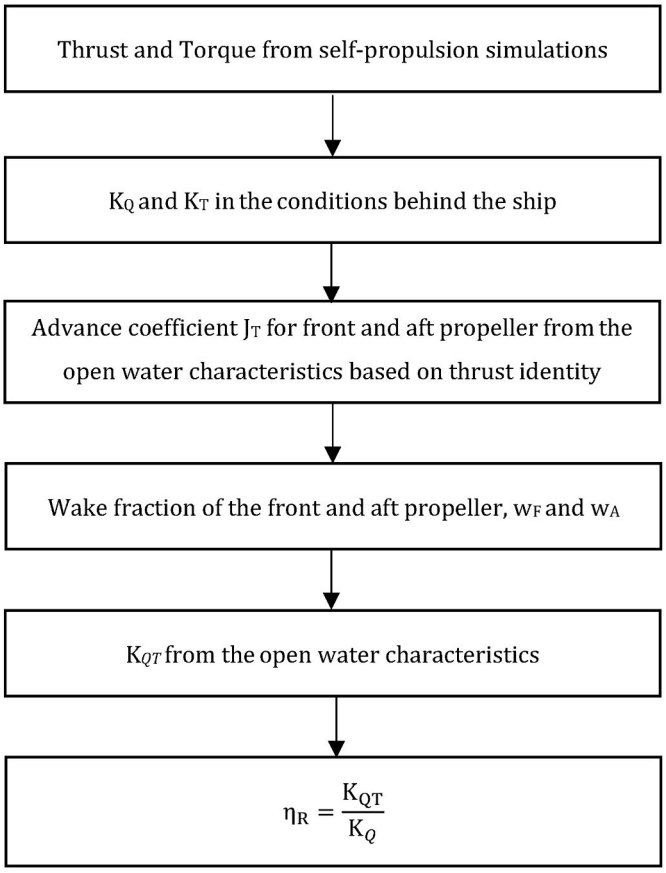

Fig. 13. Block-scheme for propulsion results determination.

$$\eta_D = \eta_0 \eta_R \frac{1-t}{1-w} \tag{16}$$

where η_0 and η_R are the open water propeller and relative rotational efficiencies respectively, while w is the wake fraction.

Since the simulations were done for the same values of the water kinematic viscosity, no correction for the differences in the calm water and propulsion simulations were introduced like suggested in ITTC procedures. This approach has been taken for all the three scales. Additionally, the values obtained from the model scale calculations have been extrapolated and these results were compared to the full scale numerical simulations.

The numerical mesh was as similar as possible to the resistance calculations to minimise the influence of the mesh itself on the results. Therefore, the mesh on the hull surface, in terms of mesh cells size and distribution was analogous to the mesh in the double body simulations. However, for more accurate wake computations the additional refinement in the area of the shaft exit and propellers was added. The mesh resolution of the propellers was analogous to the open water simulations in the crp configuration. It means that the base size of the mesh element, cells sizes on the surface of the propeller blades and hub and resolution within the area of propeller boundary layer were the same. Fig. 14 shows the mesh in the region of the propellers used for the full scale simulations.

The total mesh count for the model scale simulations for $\lambda = 37.416$ was equal to 5.3 M cells for the hull region, in the 4.8 M cells in the front propeller region, and 3.6 M cells in the aft propeller region. For the model scale $\lambda = 24$ the mesh in the static hull region had 5.5 M elements, 4.8 M cells in the rotating region of the front propeller, and 3.6 M cells in the region of the aft propeller. For the full scale it was equal to 5.8 M cells for the static region of the hull, 4.8 M cells for the front propeller region, and 4.6 M cells for the rotating region of the aft propeller. The total mesh count for the scale $\lambda = 37.416$ was equal to 13.7 M cells, 13.9 M cells for the scale $\lambda = 24$, and 15,2 M cells for the full scale simulations.

5.2. Towing tank extrapolation methods

As already mentioned in Section 5.1 the results of the calm water simulations, open water propeller characteristics and self-propulsion calculations for model scale were extrapolated using HSVA extrapolation procedures. The results were then compared to the results of the full scale simulations. This section aims to describe in detail applied existing extrapolation procedures.

For the open water propeller characteristics scaling the Strip Method according Streckwall et al. (2013) was used. For each stripe, the local Reynolds number due to individual circumferential velocity and chord length is calculated. The section drag coefficient is determined from the friction line for each section. This is done for both propeller Reynolds number in model and full scale. The resulting ΔC_D is then split into circumferential and axial component depending on the local pitch angle. This is then summarised to obtain ΔK_T and ΔK_Q for the whole propeller. To account for various flow regimes in towing tank tests (laminar ant turbulent) two friction lines are used.

The extrapolation of the calm water resistance was done according to classical Froude Method. The ITTC-57 skin friction line was used for calculation of the friction resistance for model and full scale ship. The overall calm water resistance for a full scale ship is calculated according to the formula:

$$C_{TS} = C_R + C_{FS} + C_A \tag{17}$$

Where C_A is the Correlation Allowance (C_A) and in this case it was equal to $C_A = -0.152 \cdot 10^{-3}$. The correction for hull roughness and aerodynamic resistance is not considered up to this point.

The prediction of the delivered power is done with the consideration of the hull roughness, air resistance and differences in model scale and full scale wake. The full scale propeller revolutions are determined based on the value of dimensionless ratio K_T/J^2, which is defined as:

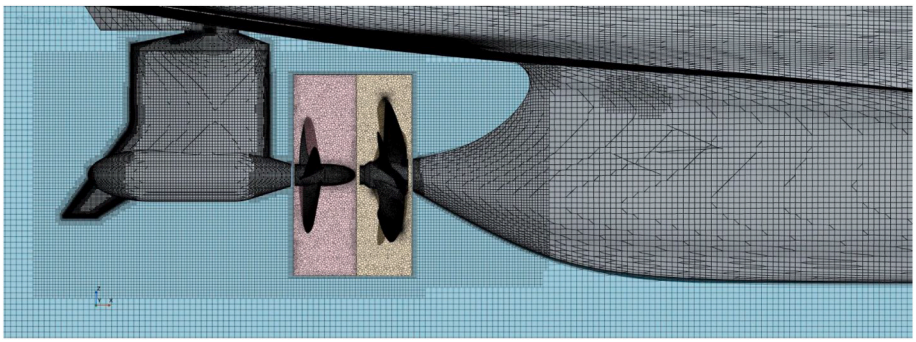

Fig. 14. Mesh for the self-propulsion calculations. Depicted: Full scale, mesh of the aft area with different mesh regions.

$$\left[\frac{K_T}{J^2}\right]_B = \frac{T}{\rho \cdot V_A^2 \cdot D^2} = \frac{T_m}{\rho_m \cdot V_{Am}^2 \cdot D_m^2} \cdot \left[\frac{1-w_m}{1-w}\right]^2 \cdot \frac{R_T + \Delta R_T + R_{AA}}{R_T} \tag{18}$$

The subscript m indicates that given value corresponds to model scale results, and where:

ΔR_T – additional resistance due to hull roughness [N].

R_{AA} – air resistance [N}

ρ – water density [kg/m^3].

The actual advance ratio J is determined by interpolating the open water characteristics in form of $(K_T/J^2)_O$ versus J curve using the $(K_T/J^2)_B$ value. The propeller revolution and total delivered power is then calculated as:

$$n = \frac{V(1-w)}{D \cdot J} \tag{19}$$

$$P_D = 2\pi \cdot n \cdot Q = 2\pi \cdot n^3 \cdot \rho \cdot D^5 \cdot \frac{K_{Q0}}{\eta_R} \tag{20}$$

The correction of the wake fraction was done based on the Yazaki method (Yazaki, 1969) and in this case term $\frac{1-w_m}{1-w}$ was equal to 1.075. Since the correction was done for the twin-skeg vessel, for the estimating the correction only half of the ship beam was taken. The results of the CFD model scale calculations were extrapolated using this procedure and compared with the full scale CFD simulation results.

6. Results

6.1. Calm water and double body simulation

The results of the resistance simulations with and without the presence of the free surface are summarised together in this section. In Table 7 the values of total, friction and pressure resistance coefficients are compared. Moreover, the values of wave resistance coefficients and form factor are shown.

Depending on the extrapolation method (classical Froude or Hughes-Prohaska) it is assumed that either:

- $C_{P\ MODEL} = C_{P\ SHIP}$ (Froude method) or,
- $C_{W\ MODEL} = C_{W\ SHIP}$ **and** $(1+k)_{MODEL} = (1+k)_{SHIP}$ (Hughes-Prohaska method)

It can be noticed that, as for the pressure resistance coefficient and (1 + k) the differences are not that significant, but the wave resistance coefficient of the full scale ship is 21% higher than for the model scale of 37.416 and 15% higher than for scale of 24. It has to be also mentioned, that this difference is somehow balanced by the lower form factor for full scale. Moreover, the wave resistance in this case is very slight part of the total resistance, therefore, even such a significant difference in coefficient value would not have a significant impact on the difference between extrapolated and computed directly total resistance.

To have a direct comparison of resistance prediction both from model tests and CFD computations, the same extrapolation method has been applied, thus values of the CFD calculations were treated as equivalent to model tests. The calm water resistance extrapolation was done following the procedure described in Section 5.2. The result of extrapolation from towing tank tests and model scale computations together with full scale simulations are presented in Table 8.

The explanation and visualisation of the differences between the wave resistance for various scales are presented in Figs. 15 and 16, which compare the wave pattern of full scale ship with model scale of 24 and 37.416, respectively. To enable the comparison, the free surface elevation was normalised by the hull length.

It can be easily noticed that the wavelength is the same for all scales, but the elevation is different. The difference between wave crests and troughs are getting more pronounced as the scale of the model decreases. It particularly applies to transverse waves since the divergent bow waves are similar for all scales.

Table 8
Comparison of towing tank and CFD calculations – resistance coefficients.

Method	CFD			EFD
Scale	1	24	37.416	
C_{TM}	–	$2.906 \cdot 10^{-3}$	$3.120 \cdot 10^{-3}$	$3.267 \cdot 10^{-3}$
$C_{FM\text{-}ITTC}$	–	$2.477 \cdot 10^{-3}$	$2.747 \cdot 10^{-3}$	$2.747 \cdot 10^{-3}$
C_R	$6.11 \cdot 10^{-3}$	$4.290 \cdot 10^{-4}$	$3.728 \cdot 10^{-4}$	$5.195 \cdot 10^{-4}$
$C_{FS\text{-}ITTC}$	$1.314 \cdot 10^{-3}$	$1.314 \cdot 10^{-3}$	$1.314 \cdot 10^{-3}$	$1.314 \cdot 10^{-3}$
C_{TS}	$1.925 \cdot 10^{-3}$	$1.591 \cdot 10^{-3}$	$1.535 \cdot 10^{-3}$	$1.681 \cdot 10^{-3}$

Table 7
Results for all scales calm water & double body simulations – resistance coefficients.

Scale	1		24		37.416	
Method	Calm water	Double body	Calm water	Double body	Calm water	Double body
C_T	$1.925 \cdot 10^{-3}$	$1.481 \cdot 10^{-3}$	$2.906 \cdot 10^{-3}$	$2.520 \cdot 10^{-3}$	$3.120 \cdot 10^{-3}$	$2.754 \cdot 10^{-3}$
C_F	$1.329 \cdot 10^{-3}$	$1.314 \cdot 10^{-3}$	$2.286 \cdot 10^{-3}$	$2.253 \cdot 10^{-3}$	$2.503 \cdot 10^{-3}$	$2.463 \cdot 10^{-3}$
C_P	$5.959 \cdot 10^{-4}$	$1.683 \cdot 10^{-4}$	$6.202 \cdot 10^{-4}$	$2.661 \cdot 10^{-4}$	$6.165 \cdot 10^{-4}$	$2.975 \cdot 10^{-4}$
C_W	$4.437 \cdot 10^{-4}$	–	$3.866 \cdot 10^{-4}$	–	$3.659 \cdot 10^{-4}$	–
(1 + k)		1.07		1.12		1.12

Table 9
Results of the self-propulsion simulations: thrust and torque of the propellers behind the ship.

Scale	n_F	n_A	$Thrust_F$	$Thrust_A$	$Torque_F$	$Torque_A$
1	1.36 rps	1.86 rps	1066 kN	590 kN	1445 kNm	670 kNm
24	6.14 rps	8.39 rps	68.35 N	36.76 N	3.934 Nm	1.820 Nm
37.416	7.50 rps	10.25 rps	17.55 N	9.53 N	0.658 Nm	0.303 Nm

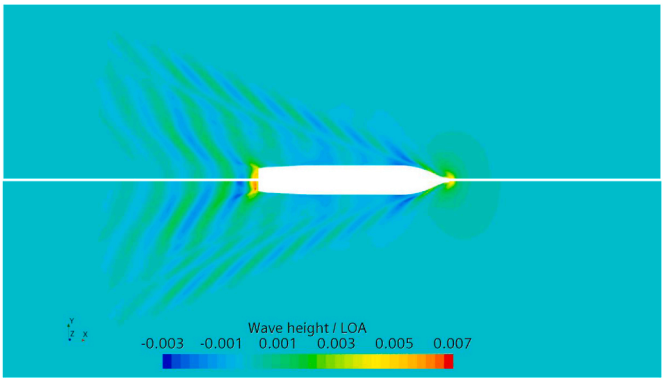

Fig. 15. Wave pattern – scale factor of 24 (top) and full scale (bottom).

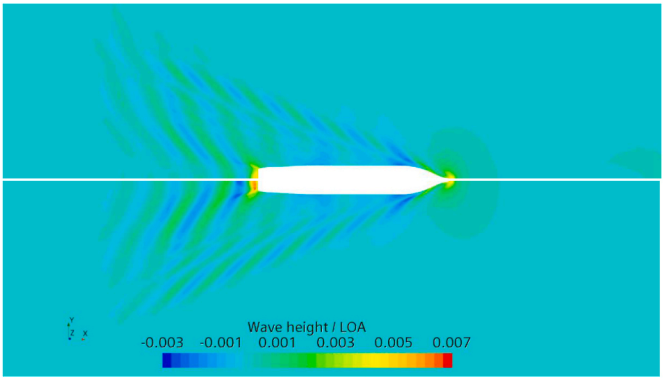

Fig. 16. Wave pattern – scale factor of 37.416 (top) and full scale (bottom).

6.2. Open water propeller characteristics

This section presents the open water propeller characteristics of the front and aft propellers for all scales, in two configurations:

- propellers analysed separately,
- contra-rotating configuration.

Fig. 17 presents the comparison of the front propeller characteristics operating separately and in crp condition. On the left are the plots for the scale of 37.416, in the middle for scale of 24, and on the right is the full scale propellers characteristics. Fig. 18 presents the same type of comparison, however, for the aft propeller. By looking from the left to the right at each propeller we can notice how the scale influences the open water propeller characteristics. It is the most interesting to notice that according to Fig. 17 the differences between efficiency of the front propeller in separated and crp conditions decrease, as the propeller Reynolds number increase. According to Fig. 18 the differences between characteristics of the aft propeller in separated and crp conditions are significant. It can also be noticed, how the propeller peak efficiency is shifted towards higher advance coefficients. This might be the effect of increasing Reynolds number, thus also increasing turbulences and reducing the boundary layer on the blades.

Fig. 19 shows in the more direct way the influence of the scale on the propellers characteristics in the open water separated conditions. The characteristics of the front propeller are presented in the plot on the right, while plot on the left shows the characteristics of the aft propeller. Additionally, in case of front propeller, the results of model tests with a propeller built to a scale of 24.98 are included. The tests were conducted for the propeller Reynolds number within a range between $6.228 \cdot 10^5$and $6.963\ 10^5$. Fig. 20 presents similar comparison of the propeller Reynolds number impact on the propeller characteristics, however, in crp conditions. The characteristics of the front propeller are presented in the plot on the left, whereas plot on the right shows the characteristics of the aft propeller.

Fig. 21 presents the comparison of the full scale CFD calculations that determined the open water propeller characteristics with the extrapolation to full scale. The subject of extrapolation were the open-water propeller characteristics for propellers in scale of $\lambda = 24$ and $\lambda = 37.416$, as they are presented in Fig. 19.

According to Figs. 19 and 20 the expected effect of increasing propeller efficiency with increasing Reynolds number can be noticed. For propeller analysed separately, the main reason for this is increased torque for larger scale propellers. It can be also seen that thrust of the front propeller is very well predicted by the CFD, however, the torque is slightly underestimated comparing to tank test results.

For the front propeller in crp configuration, the torque is almost independent on the scale, and increased propeller efficiency at higher Reynolds number is mostly due to increased thrust coefficient.

According to Fig. 21 there is good agreement between the extrapolated results and the full scale CFD calculation for the front propeller in terms of thrust and torque coefficient. The differences in the efficiency are a bit more pronounced, but it is understandable, since for the peak values of the efficiency, it is sensitive to any minor differences in the thrust and torque. For the aft propeller, the differences are more clear, but still for the advance coefficient between 0.7 and 0.8 which is around the operational point for the aft propeller the variations are not so pronounced.

6.3. Self-propulsion calculations and extrapolation

All the self-propulsion simulations were run in the same way. At the first stage, until the thrust was stabilised, the time step was one order of magnitude larger than the target time step. Then the time step was decreased to meet the propeller rotation angle per one time step requirement. Then the calculations were run to capture sufficient time for averaging ship resistance, and propeller thrust and torque. Then depending on the value of balance between resistance, thrust and friction deduction force the propeller rotation was increased or decreased.

As mentioned before, the first part of the self-propulsion simulations was determination of the optimum propeller revolutions for four different combinations of propeller rps ratios. This has been done similar to standard towing tank practice, i.e. self-propulsion point has been found for various n_A/n_F ratios between 1.2 and 1.5 and the total delivered power has been calculated. For optimum revolution ratio of $n_A/n_F = 1.366$ the final calculations for all analysed scales were performed. Table 9 presents the direct output of the simulations which are propellers revolutions, thrust and torque.

Based on the results presented in Table 9 the values of K_T and K_{QT}, i.e. thrust and torque for thrust identity for conditions behind the ship were calculated. Moreover, values of thrust deduction fraction are also included for models of various scales. At this point an interesting finding might be made, namely according to results shown in Table 10 the values of thrust deduction fraction are heavily dependent on the model scale. It can be seen that the differences are rather significant, indicating that the thrust deduction fraction may not be attributed only to the

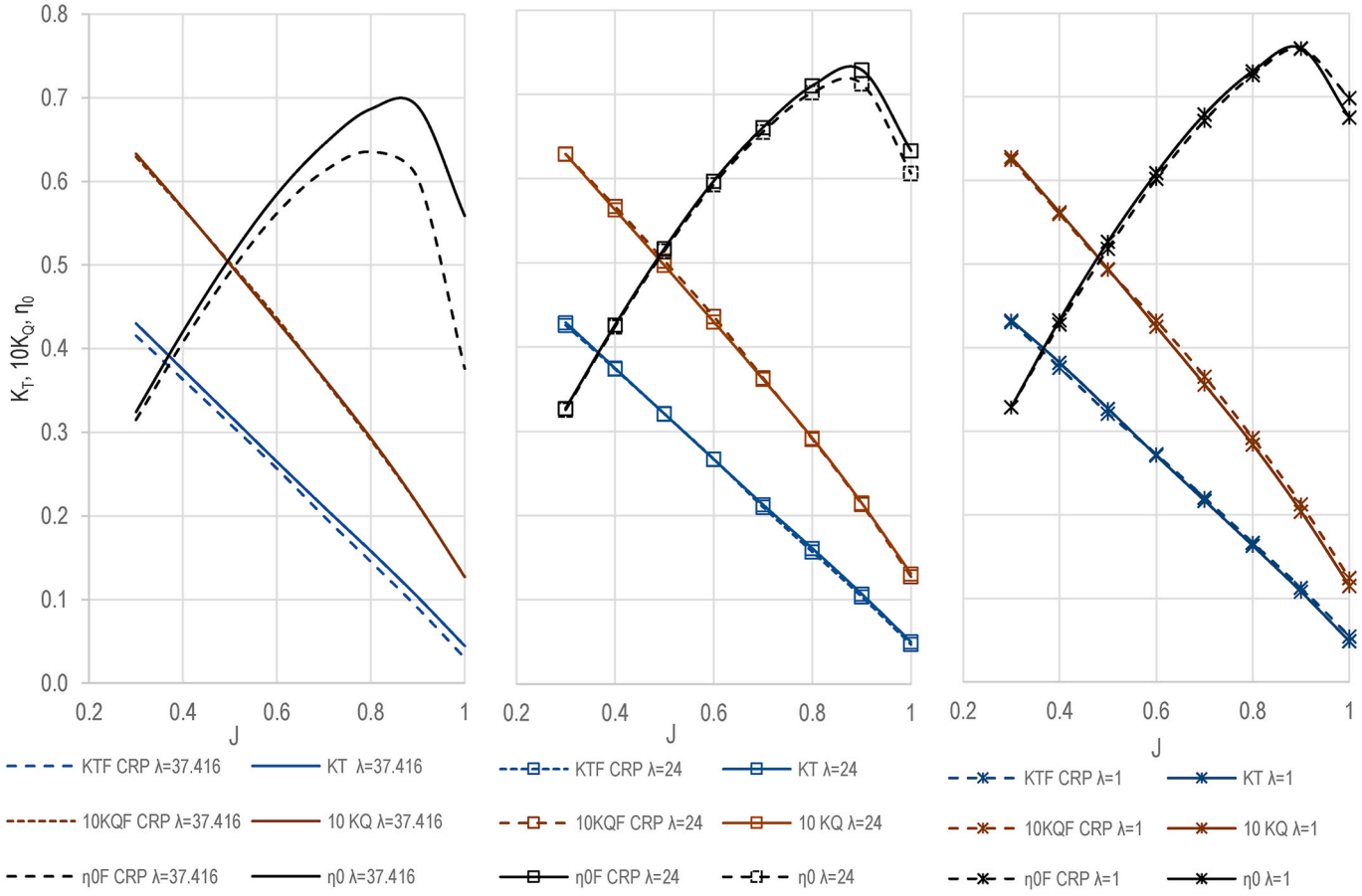

Fig. 17. Front propeller hydrodynamic characteristics for open water vs. crp configuration.

increase of the pressure resistance as we tend to assume.

Finally, the remaining steps described in propulsion parameters prediction procedure shown in Fig. 13 were taken to calculate remaining components of the propulsion efficiency. They were calculated in two ways. The first, for determination of the propellers wake fractions and rotational efficiency, used the open water propeller data in the separated condition (as presented in Fig. 19). The second used the propeller open water data in crp conditions (according to Fig. 20). Results of the first approach are presented in Table 11 and the later in Table 12.

Eventually, the values of propulsive efficiency according to Eq. (13) has been calculated. Again, the two approaches were compared, when values of the propulsive efficiency components are elaborated based on open water propeller characteristics in two conditions. It has to be noted, that open water propeller efficiency in contra-rotating system was calculated according to Equation (21):

$$\eta_{0\ CRP} = \frac{K_{T0\ CRP}}{K_{Q0\ CRP}} \frac{J_F}{2\pi} \tag{21}$$

where $K_{T0\ crp}$ and $K_{Q0\ crp}$ were calculated according to Eq. (2) and Eq. (3) and values of thrust and torque coefficients for front and aft propeller were taken from Tables 11 and 12. The rotational efficiency was calculated according to the formula:

$$\eta_{R\ CRP} = \frac{K_{Q0\ CRP}}{K_{Q\ CRP}} \tag{22}$$

Hull efficiency was calculated based of the values of front propeller wake fraction. The final results of propeller open water efficiency, relative rotational efficiency, hull efficiency and quasi-propulsive efficiency are presented in Table 13.

According to Table 13 both approaches provide relatively similar values of propulsive efficiency regardless of scale. It is quite interesting to notice that despite the differences in the values of individual components of propulsion efficiency for various scales, the propulsion efficiency as such changes in little amount.

Traditionally, the open water characteristics of crp system are presented with regards to advance coefficient calculated based on the revolution and diameter of the front propeller – see Eq. (1). Usually, the actual advance coefficient and wake field in which the aft propeller is operating is either ignored or difficult to assess. Due to large possibilities of CFD post-processing visualisations, there is an opportunity to check the wake field in multiple planes along the flow stream, including the sections between propellers.

Fig. 22 presents wake field for all three scales. In the first row the nominal wake fields upstream of the front propeller are presented. In the middle row the effective wakes of the front propeller are shown. The diameter of wake section planes is equal to 1.1 diameter of the front propeller. Finally, the bottom row presents the effective wake field for the aft propeller. The full scale is presented on the left, the scale of 24 in the middle column, and the scale of 37.416 on the right.

First what can be seen on the wake field for all the calculated cases is the asymmetry typical for twin-screw ships is visible. Second, the local velocity for the model scale calculations is significantly slower with regard to ship velocity than it takes place for full scale. It is especially pronounced for the nominal wake field. The presence of the propeller partially eliminates the differences between flow fields for various scales.

The negative values of the wake fraction indicate that locally the velocity of the flow is higher than velocity of the free stream. Differences between the effective wake fields of the aft propeller in various scales are much smaller than for the front propeller. Therefore, it means that

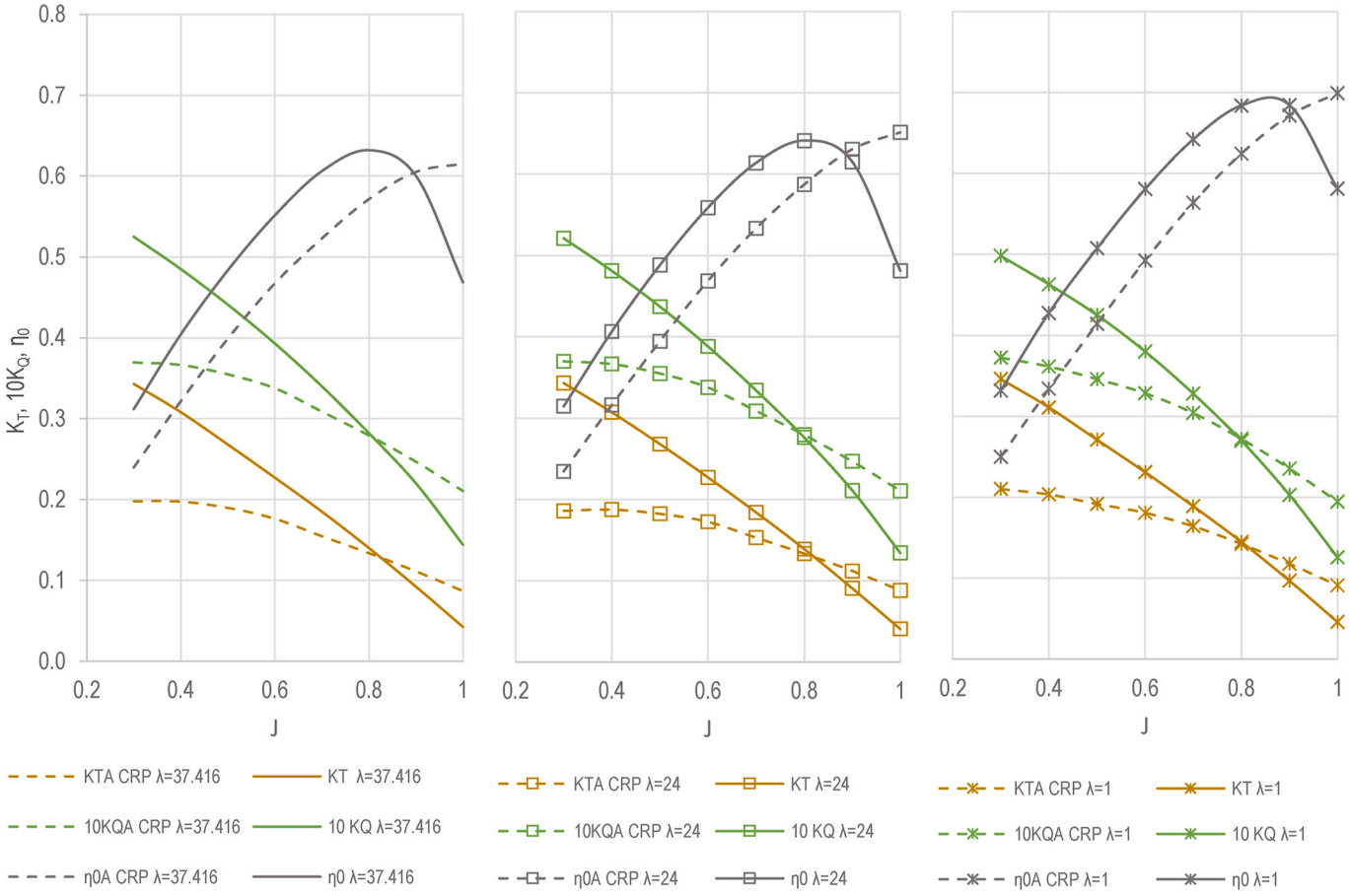

Fig. 18. Aft propeller hydrodynamic characteristics for open water vs. crp configuration.

the front propeller unifies the water inflow velocity field to the aft propeller. Nevertheless, it can be noticed that full scale aft propeller effective wake is more uniform than these calculated for the model scales.

Fig. 23 present the field function defined as magnitude of the local velocity normalised by the velocity at the inlet field function. Top picture presents the relative velocity in full scale, middle picture for the scale of 24, and bottom picture for scale of 37.416.

All three figures clearly show the difference in wake velocity between scales, especially behind the pod housing. Also, the inlet velocity to the front propeller is clearly smallest for the largest scale. It manifests itself as brighter blue colour, mixed with grey in the stern area.

Finally, the results of the model scale self-propulsion simulations were extrapolated and delivered power was compared to the one directly obtained for the full scale. Table 14 presents the comparison between the full scale CFD and extrapolation from scales of $\lambda = 24$ and $\lambda = 37.416$. Additional friction resistance due to hull roughness was added to full scale CFD results, according to HSVA procedure, and it was equal 2.5% of friction resistance. Therefore, the values are slightly different than presented in Table 9, however, they are more consistent, having similar corrections. Values in the table are given for summed up values for both propellers (on the starboard and portside).

At the first glance it can be noticed that greatest discrepancy results from values of the total resistance - extrapolated and computed directly. They are equal to −12.4 % for scale of 24 and -15.2% for the scale of 37.416 compared to full scale computations. Differences in total delivered power with regard to full scale CFD simulations are equal remarkably smaller and equal to −5.5% for scale of 37.416 and −7.4% for the scale of 24.

7. Discussion & recommendation

7.1. Calm water simulations

According to the results presented in Section 6.1 it can be seen that the convergence of the numerical solution was obtained. However, the discrepancy between value of the calm water resistance obtained from CFD and EFD is equal to almost 4.5 %. Which means, that formally according to ITTC (2021b) the calculations were not validated.

The friction coefficients obtained from the calm water numerical simulations were compared with the ITTC-57 skin friction line. The comparison is presented in Fig. 24.

It is clear that according to Fig. 24 CFD with k-ω SST model underestimates friction resistance quite significantly for model scales (−8.8% and −7.7 % for scale of 37.416 and 24, respectively). However, as the Reynolds number increase, the difference between ITTC-57 skin friction line and CFD almost disappears (1.1% for full scale). Exactly the opposite trend is observed for k- ε turbulence model, as the discrepancy increases with the model scale. The differences between friction resistance obtained by CFD and ITTC-57 friction line is a well-known issue. The influence of the skin friction line was discussed e.g. by Eça and Hoekstra (2005). Niklas and Pruszko (2019) shown that alternative skin friction lines such as numerically developed one (Eça and Hoekstra, 2008) or Grigson friction line (Grigson, 1993) are in better agreement with the CFD calculations data. Despite greater discrepancy between the CFD and towing tank data the k-ω SST model for simulations with the propellers were selected.

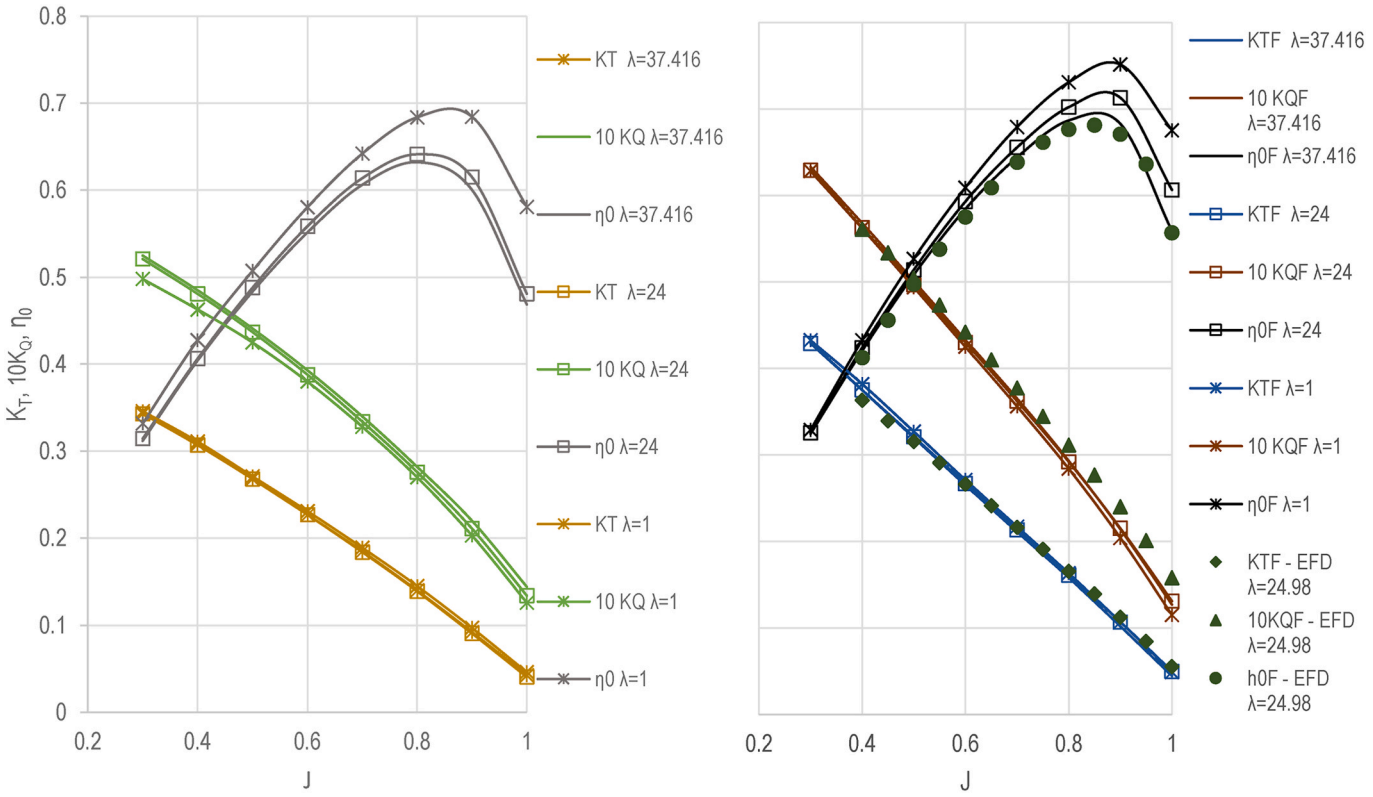

Fig. 19. Aft (left) and front propeller (right) hydrodynamic characteristics in open water conditions.

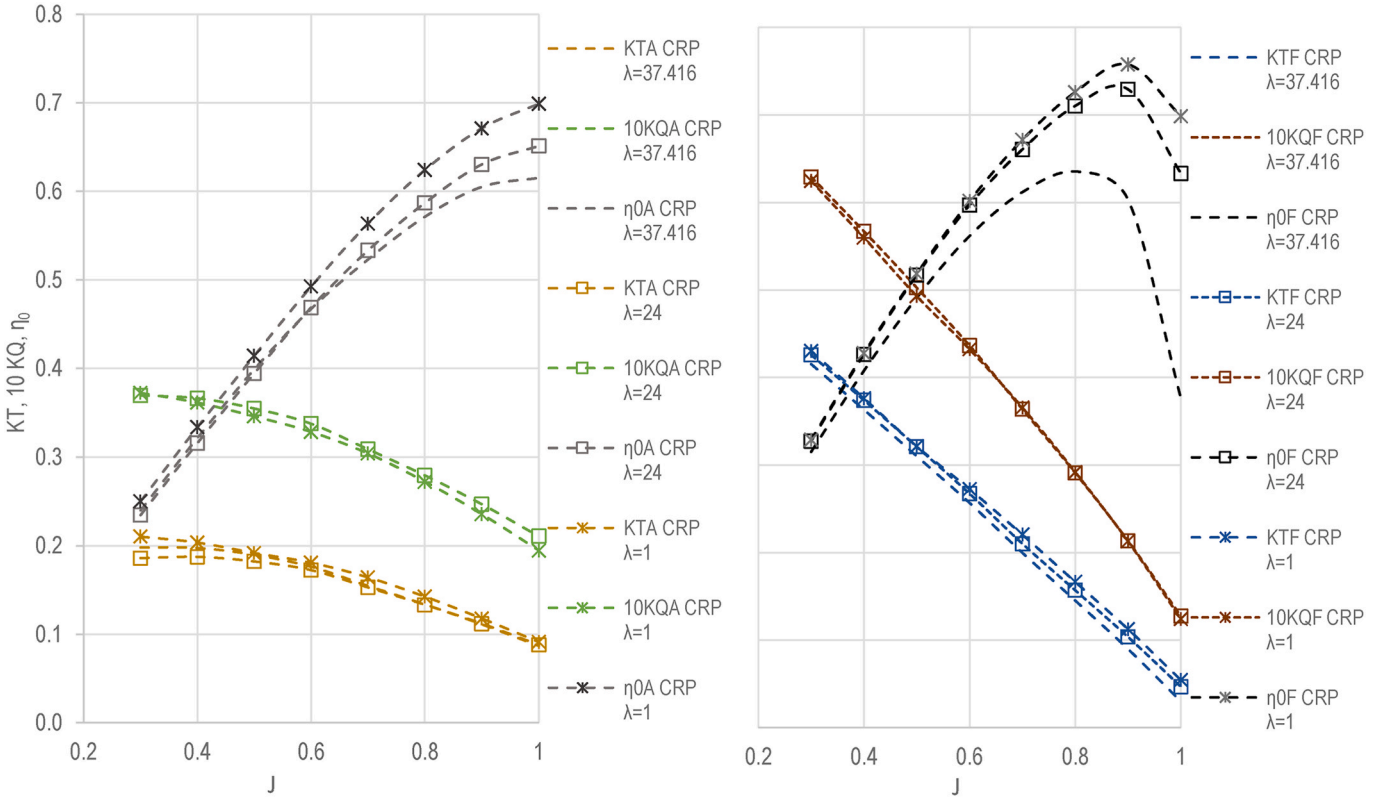

Fig. 20. Aft (left) and front propeller (right) hydrodynamic characteristics in contra-rotating configuration.

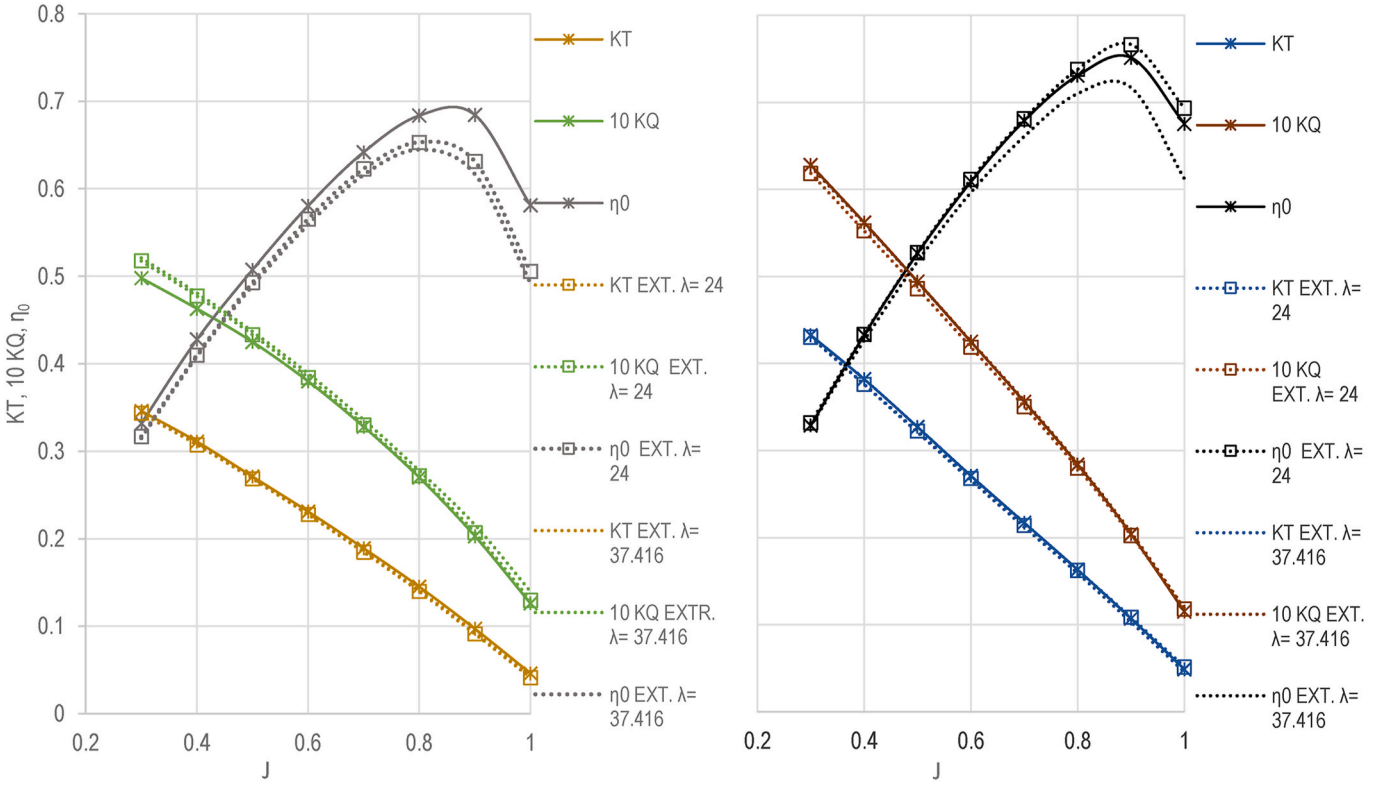

Fig. 21. Comparison of the full scale open water propeller characteristics with extrapolation from scales of $\lambda = 24$ and $\lambda = 37.416$ - aft (left) and front propeller (right).

Table 10
Results of the self-propulsion simulations: thrust and torque coefficients of the propellers behind the ship.

Scale	t	K_{TF}	K_{TA}	$10\,K_{QTF}$	$10\,K_{QTA}$
1	0.098	0.166	0.132	0.293	0.250
24	0.139	0.173	0.134	0.311	0.265
37.416	0.184	0.177	0.139	0.323	0.275

7.2. Open water propeller results

According to results presented in Section 5.1.3 and 5.1.4 first of all the extrapolation method and CFD gives very similar results, and regardless of the approach to determine the open water propeller characteristics they provide similar estimations. Therefore, the open water propeller characteristics determination and extrapolation does not seem to be crucial or questionable issue for the extrapolation method. Moreover, as already mentioned, according to Fig. 19, CFD provides very accurate estimation of the propeller characteristics.

7.3. Propulsion simulations

It is interesting to notice that according to Tables 11 and 12 the different approaches to obtain self-propulsion components (crp and separate propeller open water characteristics) does not provide quite different results of predicted pod propeller propulsive coefficients. The reason for this is the fact that according to Fig. 18 the pod propeller characteristics intersect with each other for value of advance coefficient equal to approximately $J = 0.8$. This is close to the values of advance coefficients that pod propeller operates at. The difference is the smallest for the full scale simulations.

Another aspect that requires some deeper consideration is the thrust deduction fraction. According to ITTC-78 Powering Prediction Procedure (ITTC, 2021a) the value of the thrust deduction fraction should be assumed constant for full and any model scale. According to results shown in Table 10, the values of this specific hydrodynamic interaction

Table 11
Results of the self-propulsion simulations: wake fractions and relative rotational efficiency – based on propeller open water characteristics in separate condition.

Scale	J_F	w_F	J_A	w_A	$10\,K_{Q0F}$	$10\,K_{Q0A}$	η_{RF}	η_{RA}
1	0.792	0.235	0.819	0.155	0.286	0.256	0.976	1.020
24	0.775	0.309	0.803	0.236	0.307	0.265	0.987	1.027
37.416	0.762	0.342	0.794	0.262	0.318	0.285	0.984	1.033

Table 12
Results of the self-propulsion simulations: wake fractions and relative rotational efficiency – based on propeller open water characteristics in crp condition.

Scale	J_F	w_F	J_A	w_A	$10\,K_{Q0F}$	$10\,K_{Q0A}$	η_{RF}	η_{RA}
1	0.797	0.230	0.844	0.129	0.291	0.257	0.991	1.025
24	0.770	0.313	0.811	0.228	0.312	0.278	1.003	1.051
37.416	0.740	0.361	0.788	0.268	0.335	0.286	1.036	1.039

Table 13
Results of the self-propulsion simulations: propulsion efficiency – based on propeller open water characteristics in contra-rotating condition (crp) and for separate open propeller (ow).

Scale	$\eta_{O\ CRP}$		$\eta_{R\ XRP}$		η_H		$\eta_{D\ CRP}$	
	ow	crp	ow	crp	ow	crp	ow	crp
1	0.682	0.680	0.995	1.004	1.179	1.171	**0.799**	**0.799**
24	0.644	0.628	1.002	1.022	1.247	1.254	**0.805**	**0.805**
37.416	0.626	0.588	1.003	1.037	1.238	1.275	**0.777**	**0.778**

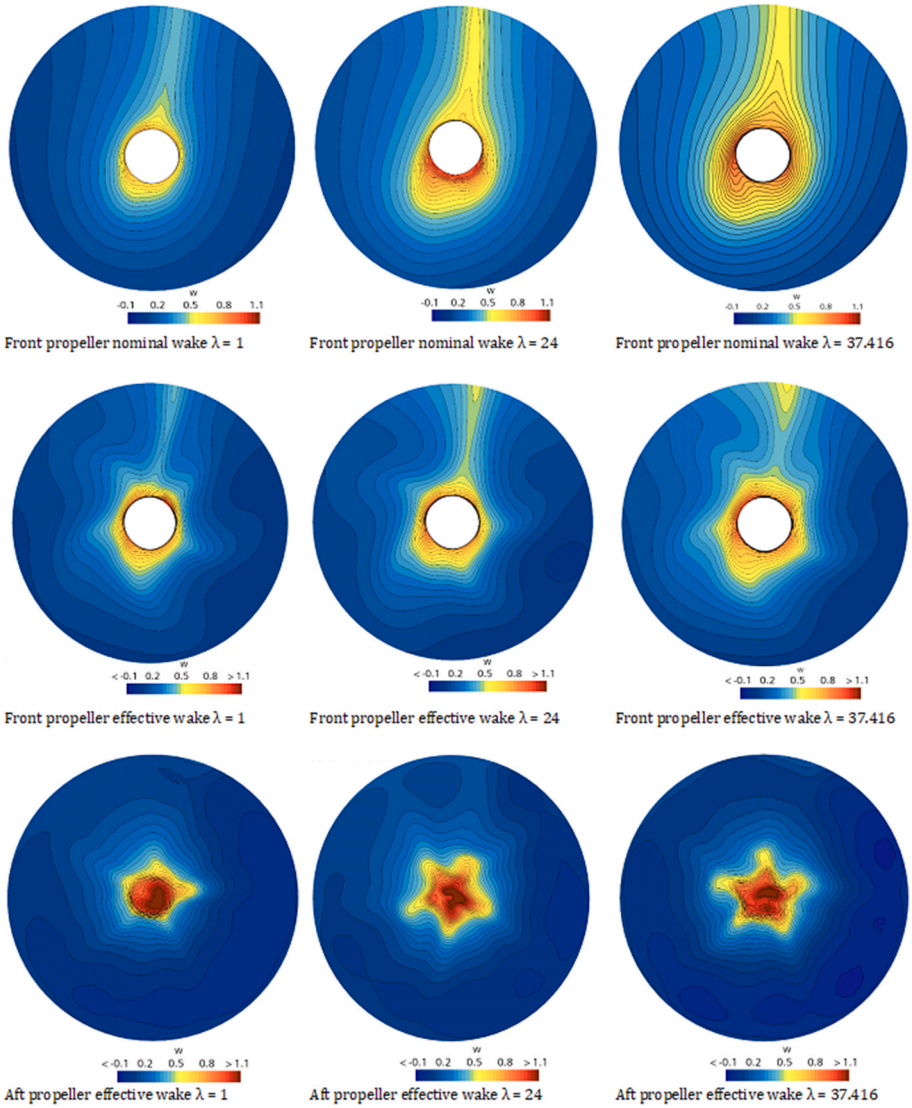

Fig. 22. Wake fields comparison - based on the axial flow velocity.

coefficient thrust deduction fraction do depend on the scale. One likely reason for the differences is lack of the pod housing in the calm water simulations, as it is taken as part of propulsion system. Therefore, the pod housing contribution to the total resistance varies. To check this issue, the resistance breakdown for all tested scales is presented in Table 15. The values of the bare hull resistance were taken from the double-body simulations.

It can be noticed that the difference between fraction of bare hull resistance in resistance and propulsion tests is almost scale-independent and that the contribution of the pod housing to the total resistance decreases with the Reynolds number.

Interestingly, the fact that the thrust deduction fraction can be scale-dependent has been discussed already by Yokoo and Taniguchi during the 11th ITTC in Tokio back in 1966 (Yokoo, K., 1966; Taniguchi, K., 1966). Both described experiments focussed on tankers, however, Taniguchi, K. (1966) indicated that the key issues from the scale effect point of view is extrapolation of the wake fraction and propeller characteristics. From the point of view of current findings, it appears that the various thrust deduction fractions are largely caused by the fact that the scale effect on the pod housing is not taken into account and is "thrown" into the thrust deduction fraction without further consideration.

Another issue is the wake fraction correction. Values of the term $(1 - w_m)/(1 - w)$ for the aft propeller is equal to 1.108 and 1.109 for scales of 37.426 and 24, respectively. For the front propeller they are equal to 1.163 and 1.141 for scales, scales of 37.426 and 24, respectively. Therefore, according to CFD, the differences between model and full

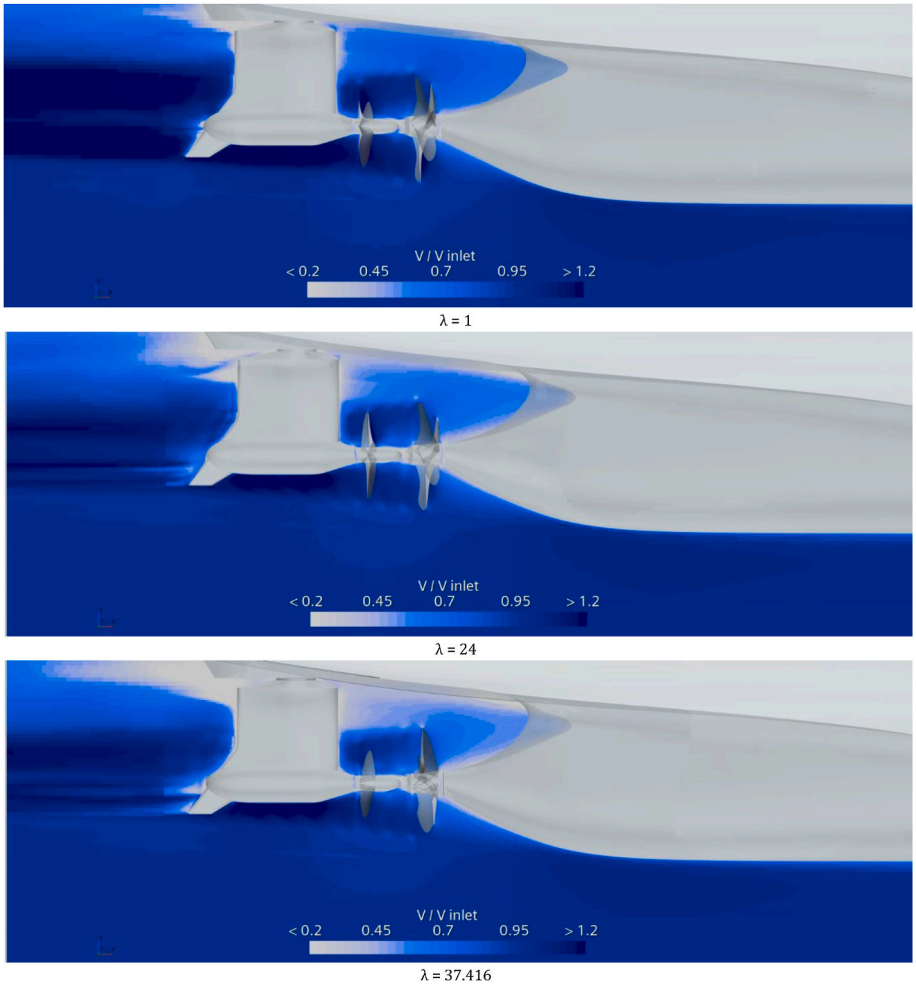

Fig. 23. Relative velocity field function at the region of the stern.

Table 14
Comparison of full scale CFD with extrapolation based on model tests and CFD results.

Quantity	Symbol	Full Scale CFD	Extrapolation from CFD λ = 24	Extrapolation from CFD λ = 37.416	Extrapolation from model tests λ = 37.416
Total resistance	R_T [kN]	2990	2620	2535	2780
Total resistance difference	[%]	0	87.6	84.8	93.0
Front propeller revolution	n_F [rpm]	81.9	78.3	77.6	79.4
Aft propeller revolution	n_A [rpm]	111.9	107.3	106.2	108.8
Front propeller thrust	T_F [kN]	2174.2	1960.4	2016.0	2239.0
Aft propeller thrust	T_A [kN]	1198.4	1067.4	1094.6	1186.1
Total delivered power	P_D [kW]	41148	38101	38869	43322
Total delivered power diff.	[%]	0	92.6	94.5	105.3

scale wake fraction are greater than according to Yazaki method. Finally, according to CFD the overall propulsive efficiency is similar for all scales.

The source of the greatest doubts and discrepancy is in the end the calm water resistance. Especially, that for the k-ω SST model, the friction resistance in the model scale is underpredicted compared to ITTC-57 line, which is the base for further extrapolation. Therefore, extrapolation of the underpredicted resistance results in lower delivered power. It is slightly balanced by the thrust deduction and lower extrapolated propeller efficiency compared to the full scale CFD. The assumption of the constant thrust in extrapolation deduction gave the value of the $\eta_D = 0.707$ for the extrapolation based on the scale of 37.416 and $\eta_D = 0.743$ for the one based on the scale of 24. According to Table 13 the value of propulsion efficiency for the full scale CFD is $\eta_D = 0.778$. Unfortunately, the full scale calm water resistance is something that cannot be validated nor compared to full scale measurements, thus it remains still as an uncertainty. It only stresses the great need for the high-quality full scale sea trials data. An action to mitigate this problem could be much more extended numerical study of different parameters, including turbulence model that influences the calm water resistance and self-propulsion results.

8. Conclusion

The paper shows the analysis of hydrodynamic performance of a hybrid crp-pod propulsion system on an Ultra Large Container Ship. The combined EFD and CFD analyses of resistance, propeller open water, propellers in crp configuration and self-propulsion performance have been conducted at different scales. For CFD computations, RANS method with k-ω SST turbulence model has been used for analyses, while for EFD

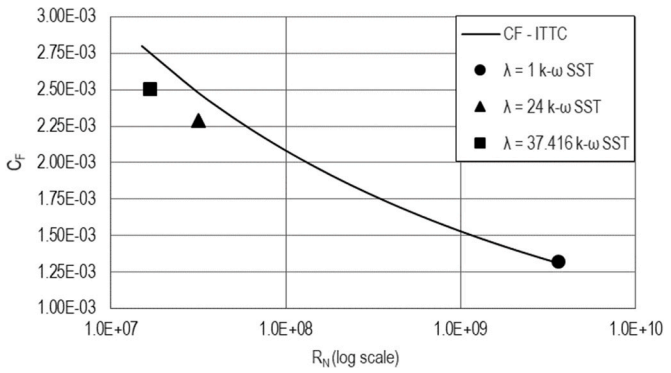

Fig. 24. Comparison of the friction coefficient for two turbulence models and ITTC-57 skin friction line.

Table 15
The comparison of the hull and pod housing resistance.

Scale	Resistance in self-propulsion		Bare hull resistance	$R_{HULL\ RESISTANCE}/R_{HULL\ PROPULSION}$	$R_{POD\ HOUSING\ PROPULSION}/R_{HULL\ PROPULSION}$
	Pod housing	Hull			
1	352.4 kN	2347 kN	2300 kN	1.020	0.098
24	30.66 N	280.65 N	275.8 N	1.018	0.110
37.416	8.064 N	82.425 N	79.56 N	1.036	0.150

standard ITTC procedures have been utilised. After the research two groups of conclusions may be drawn - these on numerical method and those on hydrodynamic performance of ULCS with hybrid crp-pod propulsions system.

Main conclusions on the CFD method, which might be drawn are:

- o turbulence model may significantly influence the results, especially the frictional component of resistance is affected,
- o the double-body simulation method appears to be rational compromise between quality of results and effort. It seems however that this method is more reliable for small scale computations,
- o as a future research, it would be beneficial to perform self-propulsion calculation with the free surface to verify the assumption of adding the wave resistance to viscous resistance obtained from double-body calculations,
- o the determination of the calm water resistance and self-propulsion point in full scale requires more attention and careful sensitivity study including mesh, time step and other turbulence models,
- o full scale CFD is characterised by good agreement with extrapolated open-water propeller characteristics,
- o model scale CFD agrees well with towing tank data, showing that propeller characteristics determination and extrapolation is not the source of major differences between obtained values of delivered power.

From hydrodynamics point of view, the performed analyses proved some obvious facts, like:

- o the aft propeller and pod propulsor have little influence on hydrodynamic performance of the front propeller,
- o the wake of front propeller has an important effect on the hydrodynamic performance of the aft propeller,
- o wake fraction coefficient for both front and aft propellers increase with smaller scale, thus the design advance coefficient moves to smaller values for smaller scales and following that thrust and torque coefficients increase.

Less obvious conclusions that might be drawn are:

- o although the delivered power differs for various model self-propulsion points, the relation between front and aft propeller revolutions shows a linear tendency,
- o the thrust deduction fraction seems to be scale-dependent, and the methodology used hitherto during propulsion performance predictions should be carefully investigated,
- o independent from extrapolation approach, i.e. with hydrodynamic characteristics from separate open water or propellers in contra-rotating configuration the total propulsive efficiency seems to be similar,
- o fixed, i.e. independent on scale, friction factor for extrapolation of pod housing resistance from model to full scale might be a wrong approach, as the contribution of pod housing resistance in overall resistance increase with smaller scale.

Despite wider insight on crp propulsion system gained throughout the research, there are still some open questions regarding the methodology of hydrodynamic performance analyses of crp-pod systems that have to be solved and will be of further interest:

- o whether the optimum balance of n_A/n_F at any model scale is still optimum for full scale,
- o how the scale influences the optimum position of the pod and aft propeller against the front propeller.

The last two bullet points together with deeper insight into full scale calm water resistance will be the subject of further study. Moreover, the more realistic treatment of the pod-housing resistance extrapolation will be investigated. CFD calculations might be helpful to determine the pod housing form factor, which can possibly improve the extrapolation procedure for the ships with crp-pod propulsion system.

CRediT authorship contribution statement

Hanna Pruszko: Writing – review & editing, Writing – original draft, Visualization, Software, Methodology, Conceptualization. **Maciej Reichel:** Writing – review & editing, Validation, Supervision, Project administration, Methodology, Funding acquisition, Conceptualization. **Marek Necel:** Writing – review & editing, Methodology. **Sören Brüns:** Writing – review & editing, Investigation.

Declaration of competing interest

The authors declare that they have no known competing financial interests or personal relationships that could have appeared to influence the work reported in this paper.

Acknowledgements

This work was supported by MarTERA and co-financed by National Center for Research and Development (NCBR), Poland, under the grant agreement MARTERA-2/twin-crp-pod ULCS/1/2020 and the German Federal Ministry for Economic Affairs and Climate Action (BMWK). Calculations were carried out at the Centre of Informatics Tricity Academic Supercomputer & Network. The model tests of front propeller mentioned in Fig. 19 have been carried out by Maritime Advanced Research Centre (CTO S.A). The authors are grateful for sharing the result.

References

Ämmälä, P., 2004. CRP azipod propulsion concept-advanced cost-effective solution. " Journal of The Japan Institute of Marine Engineering 39 (9), 544–554.

Chang, B.-J., Go, S., 2011. Study on a procedure for propulsive performance prediction for CRP-POD systems. J. Mar. Sci. Technol. 16, 1–7. https://doi.org/10.1007/s00773-010-0108-8.

Dogrul, A., Song, S., Demirel, Y.K., 2020. Scale effect on ship resistance components and form factor. Ocean. Eng. 209 https://doi.org/10.1016/j.oceaneng.2020.107428.

Eça, L., Hoekstra, M., 2005. On the accuracy of the numerical prediction of scale effects on ship viscous resistance. In: International Conference on Computational Methods in Marine Engineering MARINE 2005.

Eça, L., Hoekstra, M., 2008. The numerical friction line. J. Mar. Sci. Technol. 13 (4), 328–345. https://doi.org/10.1007/s00773-008-0018-1.

Gray-Stephens, A., Tezdogan, T., Day, S., 2021. Minimising numerical ventilation in CFD simulations of high-speed planing hulls. J. Offshore Mech. Arctic Eng. 143 (3).

Grigson, C.W.B., 1993. An Accurate Smooth Friction Line for Use in Performance Prediction, vol. 135. Transactions of the Royal Institution of Naval Architects, pp. 149–162.

Hämäläinen, R., van Heerd, J., 2013. Energy saving possibilities in twin or triple propeller cruise liners. 3rd International Symposium on Marine Propulsors. (Smp'13), Launceston, Tasmania, Australia.

He, D., Wan, D., 2017. Numerical investigation of open water performance of hybrid CRP podded propulsion system. The 8th International Conference on Computational Methods (ICCM2017).

Huang, L., Pena, B., Thomas, G., 2023. Towards a full scale CFD guideline for simulating a ship advancing in open water. Ship Technol. Res. 70 (3) https://doi.org/10.1080/09377255.2023.2167537.

ITTC, 2008. Specialist Committee on Azimuthing Podded Propulsion. Final Report and Recommendations to the 25th ITTC. In: Proceedings of the 25th ITTC. Fukuoka, Japan.

ITTC, 2014. Practical Guidelines for Ship CFD Applications. In: ITTC Quality System Manual, Recommended Procedures and Guidelines.

ITTC, 2017a. The Propulsion Committee, Final Report and Recommendations to the 28th ITTC. In: Proceedings of the 28th ITTC, Wuxi, China.

ITTC, 2017b. Hybrid Contra Rotating Shaft Pod Propulsors Model Test. In: ITTC Quality Manual System. Reccomended Procedures and Guidelines.

ITTC, 2021a. 1978 ITTC Performance Prediction Method. In: ITTC Quality Systems Manual, Recommended Procedures and Guidelines.

ITTC, 2021b. Uncertainty Analysis in CFD Verification and Validation. In: ITTC Quality System Manual, Recommended Procedures and Guidelines.

Jasak, H., Vukčević, V., Gatin, I., Lalović, I., 2019. CFD validation and grid sensitivity studies of full scale ship self-propulsion. Int. J. Nav. Archit. Ocean Eng. https://doi.org/10.1016/j.ijnaoe.2017.12.004.

Khraisat, Q., Lopes, R., Persson, M., Vikstrom, M., Bensow, R., 2023. Assessing scale effects on a propeller in uniform inflow condition. In: 25th Numerical Towing Tank Symposium. Ericeira).

Kim, S.-E., Choi, S.-H., Veikonheimo, T., 2002. Model tests on propulsion systems for ultra large container vessel. In: The 12th International Offshore and Polar Engineering Conference. Kitakyushu, Japan).

Krasilnikov, V., Slettahjell Skjefstad, V., Koushan, K., Rambech, H.J., 2023. A calibration study with CFD methodology for self-propulsion simulations at ship scale. J. Mar. Sci. Eng. 11 (7) https://doi.org/10.3390/jmse11071342.

Mikkelsen, H., Steffensen, M.L., Ciortan, C., Walther, J., 2019. Ship scale validation of CFD model of self-propelled ship. In: 8th International Conference on Computational Methods in Marine Engineering, MARINE 2019.

Mikkelsen, H., Walther, J.H., 2020. Effect of roughness in full scale validation of a CFD model of self-propelled ships. Appl. Ocean Res. 99 https://doi.org/10.1016/j.apor.2020.102162.

Niklas, K., Pruszko, H., 2019. Full scale CFD simulations for the determination of ship resistance as a rational, alternative method to towing tank experiments. Ocean. Eng. 190 (October), 106435 https://doi.org/10.1016/j.oceaneng.2019.106435.

Ponkratov, D. (Ed.), 2017. Proceedings: 2016 Workshop on Ship Scale Hydrodynamic Computer Simulations. Lloyd's Register, Southampton.

Ponkratov, D., Zegos, C., 2015. Validation of ship scale CFD self-propulsion simulation by the direct comparison with sea trials results. In: Fourth International Symposium on Marine Propulsors. Texas).

Pruszko, H., Reichel, M., Czerski, K., Necel, M., Brüns, S., 2023a. Comparison of the propulsive efficiency for the Ultra Large Container Ship: single screw, twin screw, and podded contra - rotating propulsion system. 25th Numerical Towing Tank Symposium.

Pruszko, H., Reichel, M., Czerski, K., Necel, M., Brüns, S., Schmale, J., 2023b. Scale effect in the self-propulsion prediction for Ultra Large Container Ship with contra-rotating propellers. 10th Conference on Computational Methods in Marine Engineering (Marine 2023). https://doi.org/10.23967/marine.2023.123.

Quereda, R., Pérez-sobrino, M., González-adalid, J., Soriano, C., 2017. Conventional propellers in CRP-POD configuration. Tests and extrapolation. In: Proceedings of the Fifth International Symposium on Marine Propulsors (Smp'17). Finland, Espoo.

Quist, N.A., Haurum Christensen, R., Mikkelsen, H., Walther, J.H., 2023. Validation of a full scale CFD simulation of a self-propelled ship with measured hull roughness and effect of welding seams on hull resistance. Appl. Ocean Res. 141 (December), 103746 https://doi.org/10.1016/J.APOR.2023.103746.

Reichel, M., 2017. Prediction of manoeuvring abilities of 10000 DWT pod-driven coastal tanker. Ocean. Eng. 136, 201–208.

Reichel, M., Pruszko, H., Czerski, K., Necel, M., 2022. Innovative twin-crp-pod propulsion system for ultra large container ships - challenges and opportunities. In: 15th International Symposium on Practical Design of Ships and Other Floating Structures PRADS 2022. Dubrovnik, Croatia.

Sánchez-Caja, A., Pérez-Sobrino, M., Quereda, R., Nijland, M., Veikonheimo, T., González-Adali, J., Saisto, I., Uriarte, A., 2013. Combination of pod, CLT and CRP propulsion for improving ship efficiency: the TRIPOD project. In: 3rd International Symposium on Marine Propulsors. (Smp'13). Launceston, Tasmania, Australia).

Sasaki, N., Kuroda, M., Fujisawa, J., Imoto, T., Sato, M., 2009. On the model tests and design method of hybrid CRP podded propulsion system of a feeder container ship. In: 1st International Symposium on Marine Propulsors (Smp'09). Trondheim, Norway).

Siemens PLM Software, 2022. User Guide Star CCM+, 17.08.

Shimamoto, H., Takeda, A., Miyake, S., 2011. Tandem hybrid CRP (Contra-Rotating propeller) system. Journal of the Japan Institute of Marine Engineering 46 (No.3).

Stern, F., Yang, J., Wang, Z., Sadat-Hosseini, H., Mousaviraad, M., 2013. Computational ship hydrodynamics: nowadays and way forward. Int. Shipbuild. Prog. 60 https://doi.org/10.3233/ISP-130090.

Streckwall, H., Greitsch, L., Müller, J., Scharf, M., Bugalski, T., 2013. Development of a strip method proposed as new standard for propeller performance scaling. Ship Technol. Res. 60 (2) https://doi.org/10.1179/str.2013.60.2.002.

Sun, Wenyu, Hu, Qiong, Hu, Shiliang, Su, Jia, Xu, Jie, Wei, Jinfang, Huang, Guofu, 2020. Numerical analysis of full scale ship self-propulsion performance with direct comparison to statistical sea trail results. J. Mar. Sci. Eng. 8 (1) https://doi.org/10.3390/JMSE8010024.

Taniguchi, K., 1966. Study on the Scale Effect of Propulsive Performance by Use of Geosims of a Tanker. 11th ITTC, Tokyo.

Terziev, M., Tezdogan, T., Demirel, Y.K., Villa, D., Mizzi, S., Incecik, A., 2021. Exploring the effects of speed and scale on a ship's form factor using CFD. Int. J. Nav. Archit. Ocean Eng. 13 https://doi.org/10.1016/j.ijnaoe.2020.12.002.

Terziev, M., Tezdogan, T., Incecik, A., 2019. A geosim analysis of ship resistance decomposition and scale effects with the aid of CFD. Appl. Ocean Res. https://doi.org/10.1016/j.apor.2019.101930.

Ueda, N., Numaguchi, H., 2005. The first hybrid CRP-POD driven fast Ropax ferry in the world. Journal of the Japan Institute of Marine Engineering 40 (N^{o} 2) 2005. https://doi.org/10.5988/jime.40.2_209.

Van Manen, J.D., Oosterveld, M.W.C., 1968. Model Tests on Contrarotating Propellers. 7th Symposium on Naval Hydrodynamics, Rome, Italy.

Wang, R., Xiong, Y., 2018. An integral panel method for the hydrodynamic analysis of hybrid contra-rotating shaft pod propulsors. J. Ocean Eng. Sci. 3, 175–185.

Wang, Z., Xiong, Y., Wang, R., 2016a. Effect of the main design parameters on the open-water performance of a hybrid CRP podded propulsion system. Harbin Gongcheng Daxue Xuebao/Journal of Harbin Engineering University 37 (1), 98–103.

Wang, Z.-z., Xiong, Y., Wang, R., Zhong, C.-h., 2016b. Numerical investigation of the scale effect of hydrodynamic performance of the hybrid CRP pod propulsion system. Appl. Ocean Res. 54, 26–38, 2016.

Wang, Z.-z., Min, S.-s., Peng, F., Shen, X.-r., 2021. Comparison of self-propulsion performance between vessels with single-screw propulsion and hybrid contra-rotating podded propulsion. Ocean Eng. 232 (2021), 109095.

Xiong, Y., Zhang, K., Wang, Z.-z., Qi, W.-j., 2016. Numerical and experimental studies on the effect of axial spacing on hydrodynamic performance of the hybrid CRP pod propulsion system. China Ocean Eng. 30 (4), 627–636.

Yazaki, A., 1969. A Diagram to Estimate the Wake Fraction for an Actual Ship from a Model Tank Test. 12th ITTC, Rome.

Yokoo, K., 1966. Scale Effect Experiment on Tanker Models. 11th ITTC, Tokyo.

Yu, Jiawei, Wu, Zhiqi, Wang, Luqun, Zhou, Yujie, Zhang, Zhiguo, 2021. Full scale KCS self-propulsion simulation using different propulsion models. In: Journal of Physics: Conference Series. https://doi.org/10.1088/1742-6596/1834/1/012015, 1834.

Zhang, Y.-x., Wu, X.-p., Zhou, Z.-y., Cheng, X.-k., Li, Y.-l., 2019. A numerical study on the interaction between forward and aft propellers of hybrid CRP pod propulsion systems. Ocean. Eng. 186, 106084.

Zhang, Y., Cheng, X., Feng, L., 2020. Numerical investigation of the unsteady flow of a hybrid CRP pod propulsion system at behind-hull condition. Int. J. Nav. Archit. Ocean Eng. 12, 918–927.